

The Multiscale Restriction Smoothed Basis Method for Fractured Porous Media (F-MsRSB)

Sweij Shah ^{a,*} Olav Møyner ^b Matei Tene ^a Knut-Andreas Lie ^b
Hadi Hajibeygi ^a

^a*Department of Geoscience and Engineering, Faculty of Civil Engineering and Geosciences, Delft University of Technology, P.O. Box 5048, 2600 GA Delft, The Netherlands*

^b*SINTEF, Department of Applied Mathematics Forskningsveien 1, Oslo, Norway
P.O.Box 124 Blindern, N-0314 Oslo*

Abstract

A novel multiscale method for multiphase flow in heterogeneous fractured porous media is devised. The discrete fine-scale system is described using an embedded fracture modeling approach, in which the heterogeneous rock (matrix) and highly-conductive fractures are represented on independent grids. Given this fine-scale discrete system, the method first partitions the fine-scale volumetric grid representing the matrix and the lower-dimensional grids representing fractures into independent coarse grids. Then, basis functions for matrix and fractures are constructed by restricted smoothing, which gives a flexible and robust treatment of complex geometrical features and heterogeneous coefficients. From the basis functions one constructs a prolongation operator that maps between the coarse- and fine-scale systems. The resulting method allows for general coupling of matrix and fracture basis functions, giving efficient treatment of a large variety of fracture conductivities, and basis functions can be adaptively updated using efficient global smoothing strategies to account for multiphase flow effects. The method is conservative and because it is described and implemented in algebraic form, it is straightforward to employ it to both rectilinear and unstructured grids. Through a series of challenging test cases for single and multiphase flow, in which synthetic [and](#) realistic fracture maps are combined with heterogeneous petrophysical matrix properties, we validate the method and conclude that it is an efficient and accurate approach for simulating flow in complex, large-scale, fractured media.

Key words: Fractured porous media, embedded fractured modelling, multiscale finite-volume methods, restriction smoothed basis, algebraic iterative multiscale solver, scalable linear solvers, multiphase flow, reservoir simulation.

1 Introduction

Accurate simulation of multiphase flow in natural porous media represented on high-resolution numerical grids is computationally demanding. Fine-scale petrophysical properties like permeability are often highly heterogeneous, change over several orders of magnitudes, and, in general, do not entail scale separation [1]. This computational challenge has motivated the development of several multiscale methods, which solve accurate coarse-scale systems constructed by the use of locally-computed basis functions [2–13]. Once the coarse-scale system is solved, its solution is interpolated into the original fine-scale resolution using the sub-resolution of the basis functions. Among the proposed multiscale methods, multiscale finite-volume (MSFV) methods not only provide mass-conservative solutions at fine-scale, which is a crucial property for convergent solution of transport equations, but also enable relatively simple inclusion of the type of multiphase flow equations seen in contemporary reservoir models [3,14–19].

Multiscale methods compute approximate solution having the original fine-scale resolution so that their error (or residual) can be calculated with respect to the fine-scale discrete system. As such, one can achieve systematic strategies for reducing the error through iterative procedures that combine the multiscale solver with a fine-scale smoother [20–23]. Iterative multiscale methods are scalable and deliver mass-conservative solutions after any MSFV stage. The latter property makes them unique compared with alternative advanced solvers, such as multigrid methods [24]. Recent developments of the MSFV method include extensions to compressible and compositional nonlinear displacements [25,26], unstructured grids [11,27] and fully-implicit simulations [28]. While these important developments, combined, cast a promising framework for next-generation simulators, they have been focused mainly on addressing challenges due to complex fluid physics, highly heterogeneous rock properties, and complex computational mesh geometries.

Many geological formations—including hydrocarbon reservoirs, underground water resources, and geothermal energy production fields—are naturally fractured. Fractures are highly conductive channels which, for most practical purposes, exist in a lower-dimensional space compared to the porous matrix. Physical properties inside fractures and their length scales can be very different from those of the surrounding rock, adding significantly to the computational challenges, specially once realistic length scales and complex fracture network maps are considered. As a result, a variety of modeling approaches

* Corresponding author.

Email addresses: S.Y.Shah@tudelft.nl (Sweij Shah), Olav.Moyner@sintef.no (Olav Møyner), M.Tene@tudelft.nl (Matei Tene), Knut-Andreas.Lie@sintef.no (Knut-Andreas Lie), H.Hajibeygi@tudelft.nl (Hadi Hajibeygi).

and numerical methods for different types of fractured reservoirs have been proposed [29–42,40,43,44]. Among them, the embedded fracture modeling approach [35,36,45,46,34,47] benefits from independent grids for fracture and matrix, a promising approach for naturally fractured reservoirs and also for cases with dynamic fracture creations and closure of, e.g., geothermal systems. Note that small-scale fractures (smaller than fine-scale grid cells) are homogenized within the matrix porous rock, forming effective matrix conductivities [34]. This approach, similar to other discrete-fracture-modeling (DFM) approaches, lead to detailed fine-scale discrete systems (for matrix and fracture unknowns) with high contrasts within the entries, which are clearly much more challenging to be solved efficiently than non-fractured heterogeneous cases. Therefore, it is highly important to develop efficient multiscale methods for fractured formations.

Early attempts at developing multiscale methods for fractured media were based on a mixed finite-element formulation in which high-conductive fractures were either represented explicitly as volumetric objects [37] or the fracture-matrix interaction was modelled by the Stokes–Brinkmann equations [38,48]. Within the MSFV framework, Hajibeygi et al. [47] developed the first multiscale method for fractured porous media, in which additional fracture basis functions were introduced to map each fracture network into one coarse-scale degree-of-freedom (DOF). Later, Sandve et al. [49] used the MSFV method to develop effective coarse-scale MINC-type model for fracture networks. Very recently, Tene et al. [50,51] developed a general formulation for fractured media by proposing an algebraic multiscale solver for fractured media (F-AMS). In the F-AMS, fracture basis functions were introduced on the basis of a coarsening ratio inside fracture domain, similar as in the matrix rock. Results of F-AMS when only a few fracture DOFs were used illustrated that such a multiscale map for fractured domains is quite efficient. Similar to all MSFV and AMS methods, F-AMS relies on coarse and dual-coarse grids imposed on the provided fine-scale grid cells. While the former is used to construct mass-conservative, coarse-scale systems, the latter is employed to compute local basis functions. However, geological complexities and the use of complex grid geometries make the construction of these two coarse grids quite challenging. Recently, the multiscale restriction smoothed basis (MsRSB) method was devised to overcome this complexity [52]. The MsRSB is unique in the way the basis functions are computed, yet leads to a stable and robust treatment of complex heterogeneous coefficients [53], as well as realistic flow physics for improved and enhanced oil recovery [54,55]. It is therefore favorable to use this method as a basis when seeking to extend multiscale simulation approaches for more complex fractured media.

In this work, a multiscale restricted smoothed basis method for fractured media (F-MsRSB) is developed. Following F-AMS [50,51], F-MsRSB constructs basis functions for fractures and matrix in a general way, allowing for differ-

ent level of coupling between them. In addition to F-AMS, though, F-MsRSB constructs its multiscale formulation on the basis of the MsRSB approach. This would facilitate its extensions towards complex geometries while maintaining its efficiency for highly heterogeneous challenging scenarios such as the SPE10 comparative test case [56]. Unlike previous works, the performance of F-MsRSB is investigated for realistic fracture models with complex fracture networks. Transmissibility-weighted connectivity graphs of independent fractures are decomposed using the METIS software [57], leading to an automatic coarsening strategy for fractures. Following the traditional algebraic multiscale formulations, F-MsRSB can easily be adapted to account for complex physics such as compressibility [23] and gravity [58] as discussed in [54] for the MsRSB method. To facilitate implementation, specially for complex fracture networks, here, fracture cells are introduced into the discrete systems through non-neighboring connections (NNC).

Through several two- and three-dimensional cases with highly heterogeneous coefficients, F-MsRSB is found to efficiently compute approximate solutions of good quality. Furthermore, in order to allow for error control and reduction strategies, especially for multiphase flow scenarios, the method is combined with a fine-scale smoother, ILU(0) [59,22,23]. While low-frequency errors are resolved by the coarse-scale system in F-MsRSB, the fine-scale smoother resolves high-frequency errors, the combination of which leads to an efficient iterative multiscale solver for fractured media. These iterations are applied adaptively and infrequently just to maintain user-prescribed accuracy. Several multiphase flow cases are considered in which the adaptive iterative F-MsRSB is employed to efficiently compute high-quality solutions for the flow equations. All of these systematic single- and multiphase flow cases reveal that F-MsRSB is an efficient and versatile multiscale method for naturally fractured reservoirs with highly heterogeneous coefficients.

The paper is structured as follows. The fine-scale discrete system for flow in fractured porous media is described in Section 2. Then, in Section 3.1 and Section 3 AMS and MsRSB are revisited, respectively. The development of F-MsRSB is presented in Section 4. Numerical results for single- and multiphase flow for both 2D and 3D heterogeneous reservoirs are presented in Section 5. Finally, the paper is concluded in Section 6.

2 Governing equations and fine-scale system

Mass conservation for n_{ph} incompressible phases flowing in a porous medium reads

$$\frac{\partial}{\partial t}(\phi S_\alpha) - \nabla \cdot (\boldsymbol{\lambda}_\alpha \cdot \nabla p) = q_\alpha \quad \forall \alpha \in \{1, \dots, n_{ph}\}, \quad (1)$$

where Darcy's law is employed to replace phase velocity u_α with pressure gradient ∇p . Here, gravitational and capillary effects are both neglected. Moreover, S_α and λ_α are phase saturation and mobility, respectively. Note that $\lambda_\alpha = \mathbf{k}k_{r\alpha}/\mu_\alpha$ holds, where the positive-definite permeability tensor \mathbf{k} is typically highly heterogeneous at multiple scales. Also, relative permeability, $k_{r\alpha}$ and phase viscosity, μ_α , are given functions of primary unknowns p and S . These balance equations, along with the constraint that all phases fill the pore volume, i.e.,

$$\sum_{\alpha=1}^{n_{ph}} S_\alpha = 1, \quad (2)$$

form a well-posed system of equations for $(n_{ph} + 1)$ unknowns. Sequential approaches derive a pressure equation, which is solved first, then phase velocities are obtained to subsequently solve $n_{ph} - 1$ transport equations (1). The n_{ph} -th saturation is obtained using the constraint (2). To obtain the pressure equation, i.e.,

$$-\nabla \cdot (\lambda_t \cdot \nabla p) = q_t, \quad (3)$$

the mass-balance equations (1) are summed up and the time-dependent term (accumulation) cancels out owing to the constraint (2). Total mobility, λ_t and total source terms q_t are obtained by summing their phase-wise counterparts.

For fractured porous media, following the hierarchical fracture model approach, small-scale fractures are homogenized and represented by an effective matrix permeability $\mathbf{k}^m \in \mathbb{R}^n$, whereas fractures with larger length scales are explicitly represented with an embedded fracture modeling approach (EFM). Important is that the fracture elements can cross over matrix cells, or be confined at their interfaces. In the latter case, EFM reduces to alternative discrete fracture modeling approaches. Note that fractures are lower-dimensional manifolds owing to their small apertures, so that $\mathbf{k}^f \in \mathbb{R}^{n-1}$. In this case, the pressure equation can be expressed as

$$-\nabla \cdot (\lambda_t \cdot \nabla p)^m + \psi^{mf} = q_t^m \quad \text{on } \Omega^m \subset \mathbb{R}^n, \quad (4)$$

$$-\nabla \cdot (\lambda_t \cdot \nabla p)^f + \psi^{fm} = q_t^f \quad \text{on } \Omega^f \subset \mathbb{R}^{n-1}, \quad (5)$$

where superscripts m and f represent matrix and fracture quantities, respectively. Mass exchange between fracture and matrix cells, ψ^{mf} and ψ^{fm} , is modeled as

$$\psi^{fm} = C_I \lambda_t^*(p^f - p^m) = -\psi^{mf}, \quad (6)$$

where C_I is the fracture-matrix conductivity index [47,36]. Interaction of a matrix element i and a fracture element j is defined as

$$C_I = A_{i-j}/\langle d \rangle_{i-j}, \quad (7)$$

where A_{i-j} is the fracture plate area and $\langle d \rangle_{i-j}$ is the average normal distance between i and j . More information about embedded fracture models and the

calculation of their parameters can be found in [47]. An advantage of EFM is that the fracture and matrix grids are independent and, thus, suited for many realistic scenarios such as naturally fractured reservoirs and dynamic fracture generation and closures.

Finite-volume discretization of (4) and (5) leads to a fine-scale system of equations, $Ap = q$, for matrix and fracture pressure unknowns, i.e.,

$$\begin{bmatrix} A_{mm} & A_{mf} & A_{mw} \\ A_{fm} & A_{ff} & A_{fw} \\ A_{wm} & A_{wf} & A_{ww} \end{bmatrix} \begin{bmatrix} p^m \\ p^f \\ p^w \end{bmatrix} = \begin{bmatrix} q^m \\ q^f \\ q^w \end{bmatrix}, \quad (8)$$

where w super-index denotes external well (source) terms [1]. Obviously, A_{fw} and A_{wf} will be zero if no well is drilled into fracture domain.

The formulation of this paper is developed into the open-source Matlab simulator MRST [60,61], in which fractures are introduced using non-neighboring connections (NNC) [42,62,41] and a sequentially-implicit strategy is used to simulate multiphase flow [53,54].

3 Multiscale Restriction Smoothed Basis Method (MsRSB)

Large-scale heterogeneous formations with complex fracture network maps, along with high contrasts between fracture and matrix properties make (8) quite challenging to solve using any classical numerical method. To resolve this computational challenge, a multiscale restriction smoothed basis method for fractured media (F-MsRSB) is developed. The F-MsRSB benefits from the previously developed multiscale methods for fractured media [47,50] and the MsRSB formulation for unfractured systems [52–54]. To describe the method, we start by discussing a general algebraic multiscale formulation [22,23] before we continue to describe the specific prolongation and restriction operators of the MsRSB method. This section will cast the foundation of the next section in which the novel development of this paper, i.e., F-MsRSB, is presented.

3.1 Algebraic multiscale formulation

To avoid solving (8) directly on the fine scale, multiscale methods introduce a prolongation operator \mathcal{P} that maps between the degrees-of-freedom on the underlying fine-scale grid, that describes the (fractured) porous medium and its petrophysical parameters, and degrees-of-freedom associated with a coarse

grid partition on which we will solve the global flow problem. In other words, if p^c and p' denote approximations on the coarse and fine grids, we have

$$p' = \mathcal{P}p^c. \quad (9)$$

Note that here p' contains multiscale pressure approximations for both fracture and matrix at fine-grid resolution, i.e., $p' = [p'_m \ p'_f]^T$, while p^c contains coarse pressures for both matrix and fracture, i.e., $p^c = [p^{c,m} \ p^{c,f}]^T$. These two vectors contain $n_f = n_f^m + n_f^f$ and $n_c = n_{cm} + n_{cf}$ entries, where n_f and n_c are the number of fine cells and coarse blocks, respectively, including both matrix and fractures. To determine p^c , we introduce a restriction operator \mathcal{R} that maps the fine-scale system (8) into a coarse-scale system

$$\underbrace{(\mathcal{R}A\mathcal{P})}_{A^c} p^c = \underbrace{\mathcal{R}q}_{q^c}, \quad (10)$$

that has much smaller size (i.e., $n_c \times n_c$) than the original fine-scale system (i.e., $n_f \times n_f$), see [15]. Combining (10) and (9), the algebraic multiscale (AMS) procedure can be summarized as

$$p \approx p' = \underbrace{\mathcal{P}(\mathcal{R}A\mathcal{P})^{-1}\mathcal{R}}_{M_{ms}^{-1}} q. \quad (11)$$

In the same way, MsRSB imposes a coarse grid on top of the provided fine-scale grid. Inside each coarse grid block (coarse control volumes), a fine-scale grid cell is also selected as coarse node. Coarse blocks $\Omega_K^c \forall K \in \{1, \dots, n_c\}$ define a non-overlapping partition of the domain, where n_c is the total number of coarse blocks in the system including n_{cm} matrix and n_{cf} fracture blocks.

For the restriction operator, there are two different choices, either to use $\mathcal{R} = \mathcal{P}^T$, which will lead to a Galerkin-type formulation, or to use a finite-volume restriction procedure [3], which can be stated as discrete integration operator over coarse control volumes Ω_K^c , i.e.,

$$\mathcal{R}_{i,K} = \begin{cases} 1, & \text{if } \mathbf{x}_i \subset \Omega_K^c, \\ 0, & \text{otherwise.} \end{cases} \quad (12)$$

Here \mathbf{x}_i represents the i -th control volume at fine-scale. As shown in [52,53], the MsRSB method is not very sensitive to the choice of restriction and herein we use the finite-volume operator to ensure that we can reconstruct conservative fine-scale velocities.

The prolongation operator is constructed by solving localized flow problems, and the way these flow problems are set up varies from one method to another. However, in all multiscale methods, the prolongation operator \mathcal{P} is defined so that it stores basis function Φ_K associated with coarse block Ω_K^c in its K -th

column, i.e.,

$$\mathcal{P}_{i,K} = \Phi_K(\mathbf{x}_i) \quad \forall i \in \{1, \dots, n_f\}, \forall K \in \{1, \dots, n_c\}. \quad (13)$$

Here, $\Phi_K(\mathbf{x}_i)$ is the value of basis function Φ_K in the i -th fine-grid cell, \mathbf{x}_i . Both the original MSFV method [3] and its state-of-the-art extension (AMS) [22,23] rely on a secondary coarse partition, defined as the dual to the primal coarse grid, over which the basis functions Φ_K are locally computed. While it is possible to extend conservative multiscale methods based on a dual-grid formulation to stratigraphic and other types of unstructured grids [27,18,49,63], it has proved to be difficult, when possible, to develop satisfactory dual-primal partitions for grids with complex geometry. Moreover, localization errors induced by strong permeability contrasts across block boundaries introduce instabilities in the corresponding multipoint coarse-scale stencil. This motivated the development of a multiscale two-point flux-approximation formulation [11], in which an implicitly defined dual grid is used to compose elementary flow solutions into localized basis functions. In the MsRSB method, however, local supports for basis functions are defined based on support regions, which are relatively simple to define even for very complex grids. Once these support regions are obtained, restriction-smoothed basis functions are computed by employing a modified form of the damped-Jacobi smoothing approach, similar as in smoothed-aggregation-based multigrid methods [64–66]. In the following sections, the MsRSB support regions and basis functions are briefly explained. Detailed explanations can be found in [52,53].

3.2 Coarse grid and support regions

Basis function Φ_K can have nonzero values only in the support region I_K . For the specific case of MSFV, e.g., I_K reduces to dual-coarse grid blocks. Thus, by construction, the basis function Φ_K and consequently the K -th column of \mathcal{P} are set to zero outside I_K .

The support region of a coarse block Ω_K^c (see **Fig. 1**) is constructed by creating a local triangulation, using cell and shared-face centroids of all immediate geometrical neighbors of Ω_K^c [52]. This ensures that for a Cartesian grid without fractures, the coarse system has the same multipoint flux stencil as in the original MSFV method. Support regions for fractured coarse blocks are, because of their (potentially severe) geometrical complexities, computed by a different procedure, which will be described in the next section (see Algorithm 1).

The support boundary B_K is defined as the set of all fine cells that are topological neighbors of the outermost cells in the support region I_K . Note that $I_K \cap B_K = \emptyset$. This leads to the definition of a global boundary G which is a

union of all B_K for all $K \in \{1, \dots, n_c\}$, i.e.,

$$G = B_1 \cup B_2 \cup \dots \cup B_{n_c}. \quad (14)$$

Fig. 1 illustrates I , B and G for a 2D rectangular Cartesian and an unstructured hexagonal grid. For a Cartesian grid geometry, G becomes equivalent to the set of all dual-coarse boundary cells, i.e., similar to the classical MSFV method. Finally, indices of all support regions overlapping with each fine cell \mathbf{x}_i stored inside G are stored in the set H_i , i.e.,

$$H_i = \{K | \mathbf{x}_i \in I_K, \mathbf{x}_i \in G\}. \quad (15)$$

H_i can be visualised using the last row of images in **Fig. 1**. Note that they follow the same indexing as depicted in **Fig. 1a**. A randomly picked fine cell belonging to the global boundary G , indexed as i , and denoted by the control volume \mathbf{x}_i is depicted in blue in **Fig. 1g**. The next two images (**Fig. 1h** and **Fig. 1i**) show the support regions that encompass this control volume. Hence, the set H_i for this particular cell can be written as $H_i = \{6, 9\}$. This can be repeated for each fine cell stored inside G to generate the complete set H .

3.3 MsRSB prolongation operator

As mentioned earlier, basis function are calculated iteratively, having nonzero values only inside their support regions. The basis functions are initialized by setting each to be equal to a constant value of one inside the corresponding coarse block, i.e.,

$$\mathcal{P}_{i,K}^0 = \begin{cases} 1, & \text{if } \mathbf{x}_i \in \Omega_K^c, \\ 0, & \text{otherwise.} \end{cases} \quad (16)$$

Then, we compute the iterative increments

$$\hat{d}_K = -\omega D^{-1} A \mathcal{P}_K^\eta \quad (17)$$

where A is the fine-scale system, $D = \text{diag}(A)$ is the diagonal entries of A , and ω is a relaxation (or damping) parameter, which is set to $2/3$ for all simulations reported in this paper.

To ensure that basis functions have local support, the increments \hat{d}_K must be restricted to have nonzero values only inside I_K . This is done by setting \mathcal{P}_K^η outside the support region to zero and normalizing all other basis functions

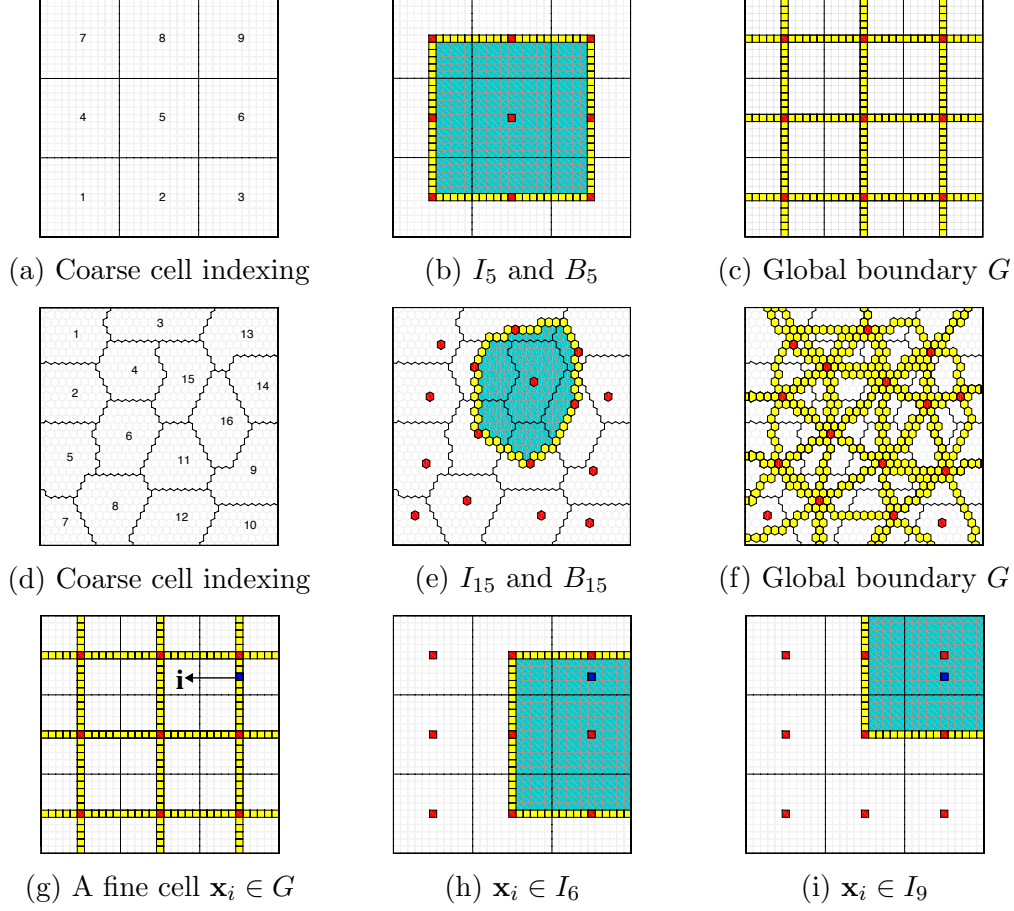


Fig. 1. The top row shows a rectangular grid with a uniform coarse partition, while the second row presents a hexagonal grid with an unstructured coarse partition. The left images (**a** and **d**) show the indexing scheme for the coarse blocks. In the middle images (**b** and **e**), cells inside the support regions for a coarse node are highlighted in turquoise, whereas yellow color signifies the support boundary. The right images (**c** and **f**) show the global boundary cells G highlighted in yellow. The last row uses the same grid as in the first row to depict the set H_i for a particular cell $\mathbf{x}_i \in G$ marked in blue (**g**). The next two images (**h** and **i**) show the support regions that make up the set H_i and contain that particular cell.

whose support region includes the boundary cells B_K , i.e.,

$$d_{iK} = \begin{cases} \frac{\hat{d}_{iK} - \mathcal{P}_{iK}^\eta \sum_{J \in H_i} \hat{d}_{iJ}}{1 + \sum_{J \in H_i} \hat{d}_{iJ}}, & \text{if } \mathbf{x}_i \in I_K \cap G, \\ \hat{d}_{iK}, & \text{if } \mathbf{x}_i \in I_K \setminus G, \\ 0, & \text{if } \mathbf{x}_i \notin I_K. \end{cases} \quad (18)$$

This modified increment is now used to update the prolongation operator, i.e.,

$$\mathcal{P}_K^{\eta+1} = \mathcal{P}_K^\eta + d_K. \quad (19)$$

To measure convergence of the basis functions, a local error e_K is defined

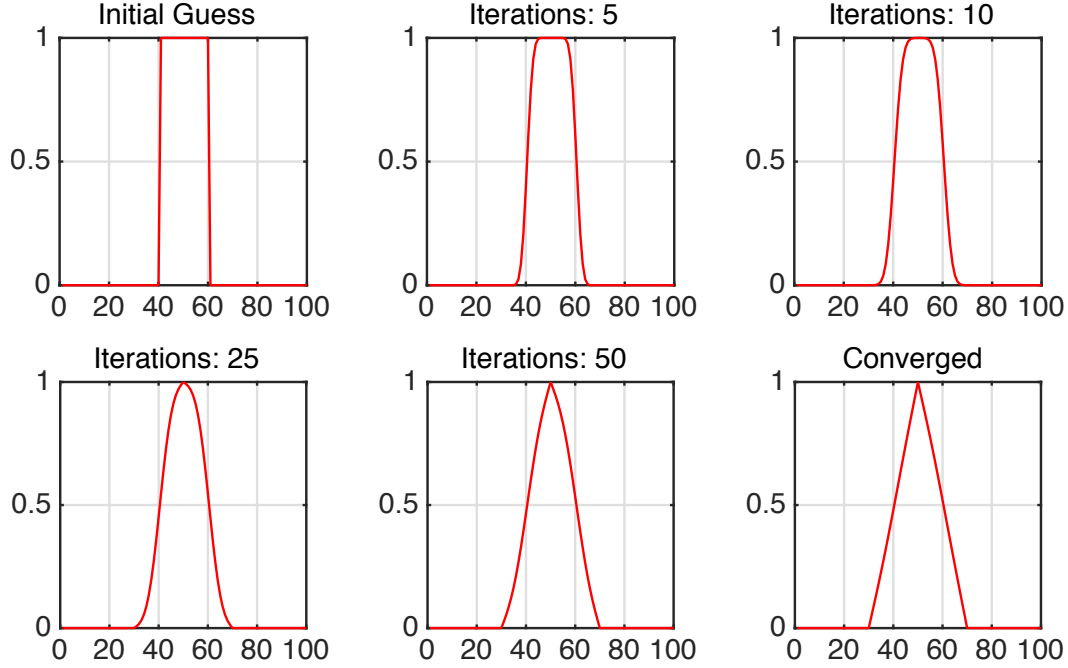


Fig. 2. Restriction smoothed basis function computed iteratively over a 100 m long 1D homogeneous domain with 20 m coarse blocks. The vertical axis gives the basis-function value for the 3rd coarse block. Tolerance for convergence = 10^{-3} .

outside G ,

$$e_K = \max_i (|\hat{d}_{iK}|), \quad \mathbf{x}_i \notin G, \quad (20)$$

and basis functions are assumed to be converged if, $\|e\|_\infty \leq \text{tolerance}$ after any increment. If not, we set $\mathcal{P}_K^\eta = \mathcal{P}_K^{\eta+1}$ and repeat the steps (17) – (19).

Note that the basis functions can be constructed using parallel processing. By virtue of the fine-scale discretization scheme used to construct the system matrix A , every successive increment computed using (17) will only spread the corresponding basis functions further by a topological distance of 1. Hence, once the basis function P_K covers its support region I_K , the next increment will spread into its support boundary B_K . Using the third expression in (18), these nonzero values outside the support region would be set to zero. This could lead to the prolongation operator not having a partition of unity. To reimpose partition of unity in the prolongation matrix, the discarded values are redistributed within other basis functions with support in these fine cells. Indices of such support regions are stored in the set H . In essence, the first and the last expression in (18) explicitly impose a partition of unity in all cells belonging to the global boundary G .

Fig. 2 shows how this iterative procedure gradually converges to the standard FEM hat function for a homogeneous 1D medium, while **Fig. 3** shows basis functions for three different 2D permeability fields.

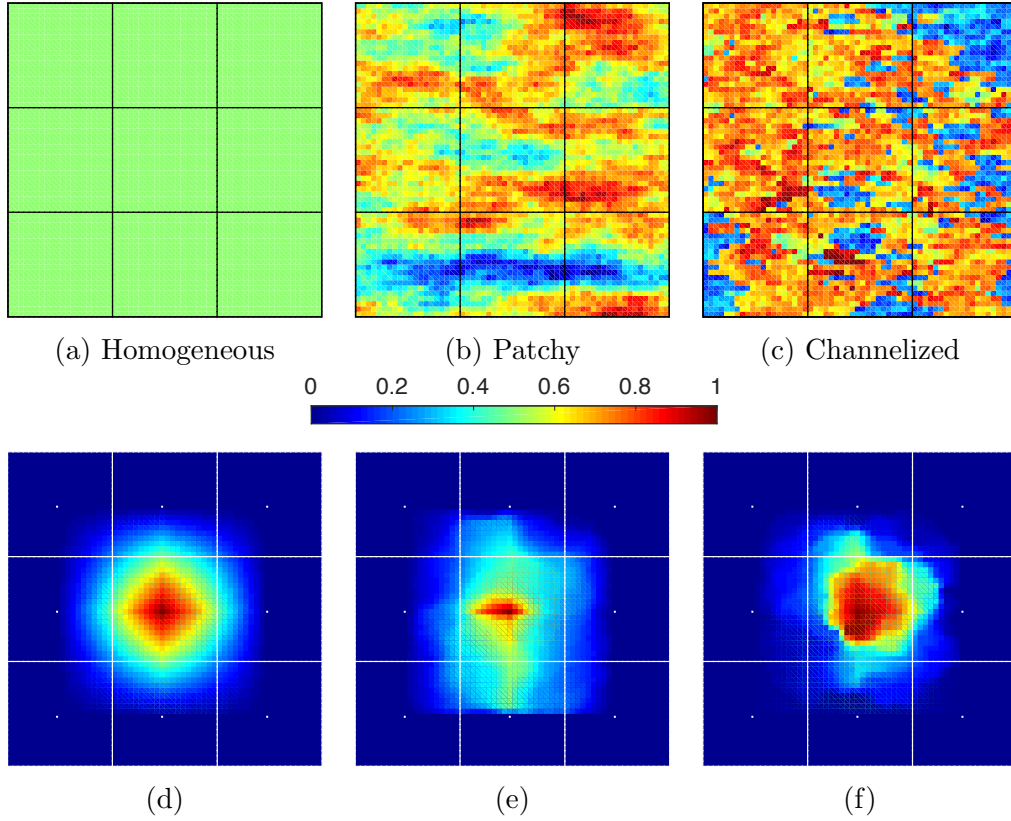


Fig. 3. Illustration of the restriction smoothed basis functions (**d-f**) for three different permeability fields: homogeneous (**a**), heterogeneous patchy-field (**b**), and heterogeneous channelized field (**c**).

4 MsRSB for Fractured Media (F-MsRSB)

The F-MsRSB method is devised on the basis of introducing basis functions for both matrix and fracture domains, similar to F-AMS [50], i.e., $p \approx p' = [p'_m \ p'_f]^T$, where

$$p'_m = \sum_{j=1}^{n_{cm}} \Phi_j^{m,m} p_j^{c,m} + \sum_{j=1}^{n_{cf}} \Phi_j^{f,m} p_j^{c,f}, \quad (21)$$

$$p'_f = \sum_{j=1}^{n_{cm}} \Phi_j^{m,f} p_j^{c,m} + \sum_{j=1}^{n_{cf}} \Phi_j^{f,f} p_j^{c,f}. \quad (22)$$

Here, p'_m and p'_f are approximate matrix and fracture pressures, respectively, computed by MsRSB at the fine scale. In addition, coarse-scale solutions in matrix and fracture are denoted as $p^{c,m}$ and $p^{c,f}$, respectively. There exist n_{cm} coarse matrix blocks and n_{cf} coarse fracture blocks in total. It is important to realise that there may be several disconnected fracture networks in a reservoir model. Each independent fracture network can contain one or more fracture coarse cells, so that n_{cf} comprises all fracture coarse blocks across

all fracture networks. Moreover, $\Phi^{m,m}$ and $\Phi^{m,f}$ are basis functions for matrix coarse blocks with superscripts m,m and m,f denoting values in the matrix and fracture domains, respectively. Both $\Phi^{f,f}$ and $\Phi^{f,m}$ are fracture basis functions with superscript f,f representing the values inside the corresponding fracture network and superscript f,m denoting contributions inside the matrix domain. Hence, the prolongation operator can be written as

$$\mathcal{P} = \left[\begin{array}{cc|cc} \vdots & \vdots & \vdots & \vdots \\ \Phi_1^{m,m} & \dots & \Phi_{n_{cm}}^{m,m} & \Phi_1^{f,m} & \dots & \Phi_{n_{cf}}^{f,m} \\ \vdots & \vdots & \vdots & \vdots & \vdots & \vdots \\ \hline \vdots & \vdots & \vdots & \vdots & \vdots & \vdots \\ \Phi_1^{m,f} & \dots & \Phi_{n_{cm}}^{m,f} & \Phi_1^{f,f} & \dots & \Phi_{n_{cf}}^{f,f} \\ \vdots & \vdots & \vdots & \vdots & \vdots & \vdots \end{array} \right]_{n_f \times n_c}, \quad (23)$$

where $n_f = (n_f^m + n_f^f)$ and $n_c = (n_{cm} + n_{cf})$ are total degrees-of-freedom (matrix and fractures) at fine and coarse scales, respectively.

Generally, fractures are much more conductive than the matrix rock. Full consideration of both fracture and matrix coarse solutions, $p^{c,m}$ and $p^{c,f}$, for interpolated fracture pressure, p'_f , can lead to improved convergence properties. However, such an approach results in much denser prolongation operators. Therefore, the improvement in convergence rate may not necessarily offset the additional computational cost. Numerical studies of F-AMS for 3D problems (considering CPU time), support the idea of eliminating the effect of matrix coarse pressure in the fracture pressure interpolation, i.e., setting $\Phi^{m,f} = 0$. In this paper, the same sparse operator is considered.

Next, the support region and the procedure for calculating basis functions for fractured media are explained.

4.1 Support regions and basis functions

The support region for each fracture block is generated based on a topological distance. More precisely, the support region for a fracture block includes all fine cells located inside the sphere (circle in 2D) with radius d in index space. Note that d is an integer input to the simulator but there is no algorithmic restriction on using expressions to automatically compute d . Optimization of the choice of fracture support regions would require a more detailed study, considering both accuracy and efficiency, and also taking into account the effective coarsening ratio used to compute the multiscale solution. Such a

Algorithm 1 Generating fracture support regions

Initialize: $A =$ Adjacency matrix for the fine-scale system, $d \in \mathbb{Z}$ and $m = 1$

- 1: **for** $J \in \{1, \dots, n_{cf}\}$ **do**
- 2: $I_{i,J} = 1$ if $\mathbf{x}_i \in \Omega_J^c$, $I_{i,J} = 0$ otherwise
- 3: **while** $m < d$ **do**
- 4: $I_J = A \times I_J$
- 5: $m = m + 1$
- 6: **end while**
- 7: **end for**

study is beyond the scope of this paper and subject of a future study. It is clear that the support region will include no fine-cell except those overlapping with the fractures, if $d = 0$ is considered. For the numerical examples studies in this paper the value of $d = 7$ is used. This is of the same order as the matrix coarsening ratio used in our examples (i.e. 10 in each direction). An overview of the procedure to generate the fracture support region is presented in Algorithm 1.

Fig. 4 illustrates coarse grids and support regions inside which basis functions are compactly supported for a test case with 30×30 matrix and 20 fracture cells. Furthermore, **Fig. 5** shows basis functions inside the matrix rock (belonging to both fracture and matrix coarse nodes).

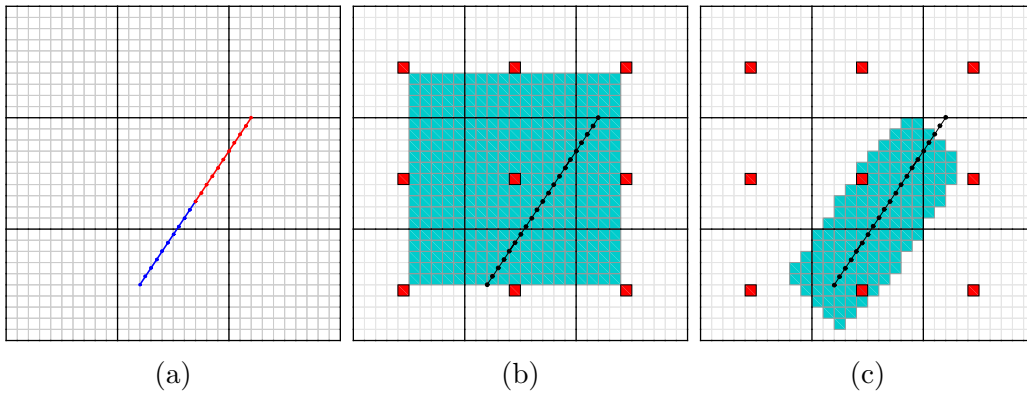


Fig. 4. Illustration of multiscale grids for matrix and fracture **(a)** with support regions for matrix **(b)** and fracture **(c)** for a case with 30×30 matrix and 20 fracture fine-scale cells. Multiscale coarse grid contains 3×3 matrix blocks and 2 blocks inside the fracture. Here, $d = 7$.

5 Numerical Results

The developed F-MsRSB method is implemented and integrated with the free, open-source Matlab Reservoir Simulation Toolbox (MRST) [61,67,68,60]. In

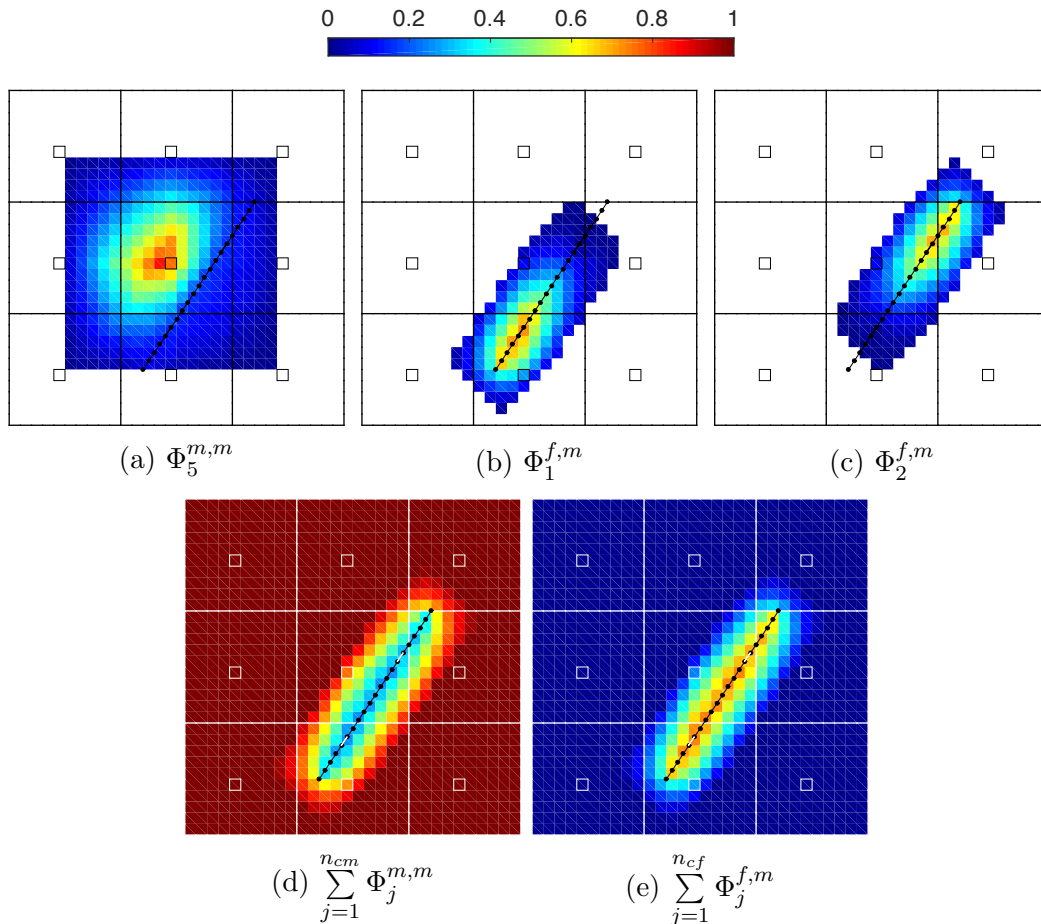


Fig. 5. Matrix and fracture basis functions for the system described in **Fig. 4**

this section, we investigate the performance of F-MsRSB for many challenging cases. The numerical examples involve both 2D and 3D heterogeneous media. Next, the sensitivity of the method to coarse-grid resolution for fracture domain is studied. Then, its performance for heterogeneous rock formations is studied through a realistic fracture map obtained from an outcrop and for a statistically generated fracture map. Using an outcrop map is unique in the literature of multiscale methods for fractured media. For the statistical map, we use METIS [57] to generate an unstructured partition of a fine-scale hexagonal grid representing the matrix rock. Finally, three test cases with 3D heterogeneous matrix properties along with 2D fracture plates are considered to provide the scientific community with a reliable assessment of the devised F-MsRSB method.

5.1 Sensitivity to coarse DOFs in fracture

In this test case, we consider single-phase flow in a $100 \times 100 \text{ m}^2$ homogeneous domain to study the effect of the coarsening ratio in the fracture domain on

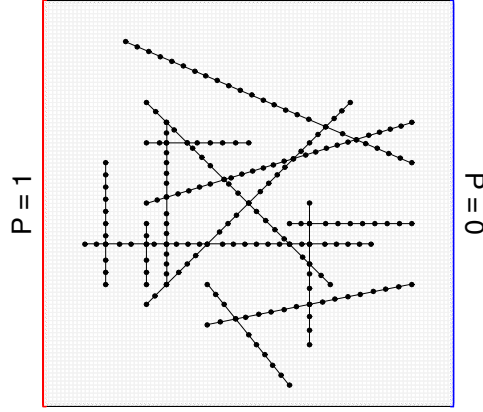


Fig. 6. First test case which contains 100×100 matrix and 200 fracture cells at the fine scale, with homogeneous 2D rock formation. The left and right boundaries are subject to Dirichlet values of 1 and 0, respectively.

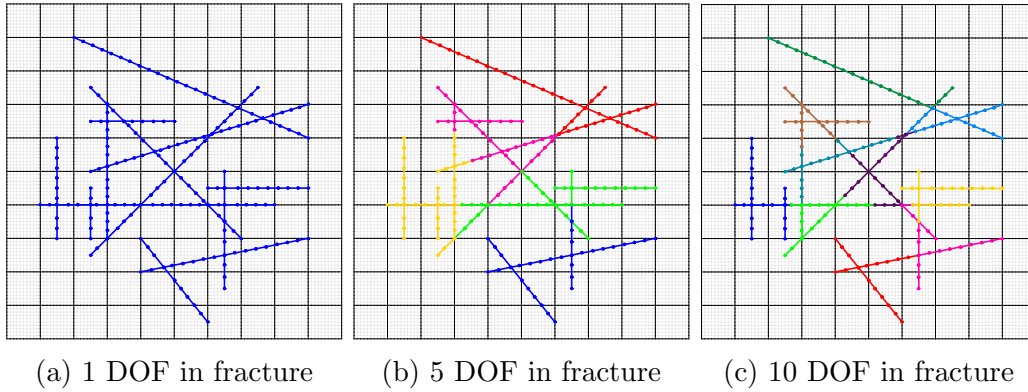


Fig. 7. F-MsRSB coarse grids for matrix and fractures. Each coarse matrix block consists of 10×10 fine cells, while the fracture blocks are varied from 1 (200 fine cells in 1 block) to 5 (40 cells in each block) and 10 (20 cells in each block).

the accuracy of the multiscale method as well as its preconditioning properties. The matrix permeability is set to 1 Darcy and $k^f/k^m = 10^4$. Fluid viscosity is 1 cP. The matrix contains 100×100 grid cells. As shown in **Fig. 6**, the matrix contains one fracture network described using 200 cells. A coarsening ratio of 10×10 is fixed for the matrix domain, while the coarsening ratio for the fracture is varied from 1 to 50 (some cases are shown in **Fig. 7**). By increasing the number of coarse degrees-of-freedom in the fracture, the F-MsRSB pressure solution improves (**Fig. 8**). This finding is consistent with that of F-AMS [50].

Fig. 8 shows pressure solutions after one multiscale cycle for different fracture coarsening ratios. As a quantitative error measurement, the F-MsRSB pressure

error is calculated using a scaled discrete L^2 norm

$$\epsilon_p = \sqrt{\frac{\sum_{i \in n_f} (p_i^{fs} - p_i^{ms})^2 |\Omega_i|}{\sum_{i \in n_f} (p_i^{fs})^2 |\Omega_i|}}. \quad (24)$$

Errors for different grid sizes inside the fracture are also provided in **Fig. 8**. In **Fig. 9**, we have used Pollock’s method [70] to trace streamlines for the fine-scale reference solution and the multiscale solution computed using different degrees of freedom in the fracture. This provides an excellent way to visualize the flow field and study the accuracy of the multiscale velocity profile. Additionally, to quantify the accuracy of the velocity field we consider a vertical slice in the middle of the matrix domain, as shown in **Fig. 10a**. The total flow rates obtained by F-MsRSB (q^{ms}) and the fine-scale discretization (q^{fs}) are compared across this section. **Fig. 10b** reports the discrepancy

$$\epsilon_q = 100 \times \frac{|q^{fs} - q^{ms}|}{|q^{fs}|}, \quad (25)$$

at this cross section as a function of fracture coarsening ratio. Similarly to F-AMS [50], we observe that the condition number of the F-MsRSB coarse system improves by increasing the coarse resolution inside the fracture. This leads to higher iterative convergence rates, as shown in **Fig. 11**, if F-MsRSB is combined with ILU(0) in an iterative multiscale procedure [50]. Convergence is determined on the basis of setting a threshold value for the scaled residual norm, i.e., $\|r_b\|_2 = \|Ap - q\|_2 / \|q\|_2$.

5.2 F-MsRSB for heterogeneous fractured media

To study F-MsRSB for heterogeneous fractured media, two fracture maps are considered: (i) the fracture map is extracted from an outcrop of dimensions 246.3×283.1 m²; (ii) a statistical fracture model is generated over an unstructured PEBI grid. The heterogeneous rock property is assumed to represent heterogeneity variations in the matrix rock along with homogenized small-scale fractures.

5.2.1 Outcrop fracture map

The fracture coordinates are scaled from an outcrop photo [69] to fit a domain size of 1000×1000 m², as shown in **Fig. 12a**. The fine-scale grid contains 100×100 matrix and 2074 fracture cells (over 94 disconnected fracture networks), while the F-MsRSB grid contains 15×15 matrix and 155 fracture blocks. **Fig. 12b** shows the permeability of the matrix formation. Fracture permeability is set to 1000 Darcy.

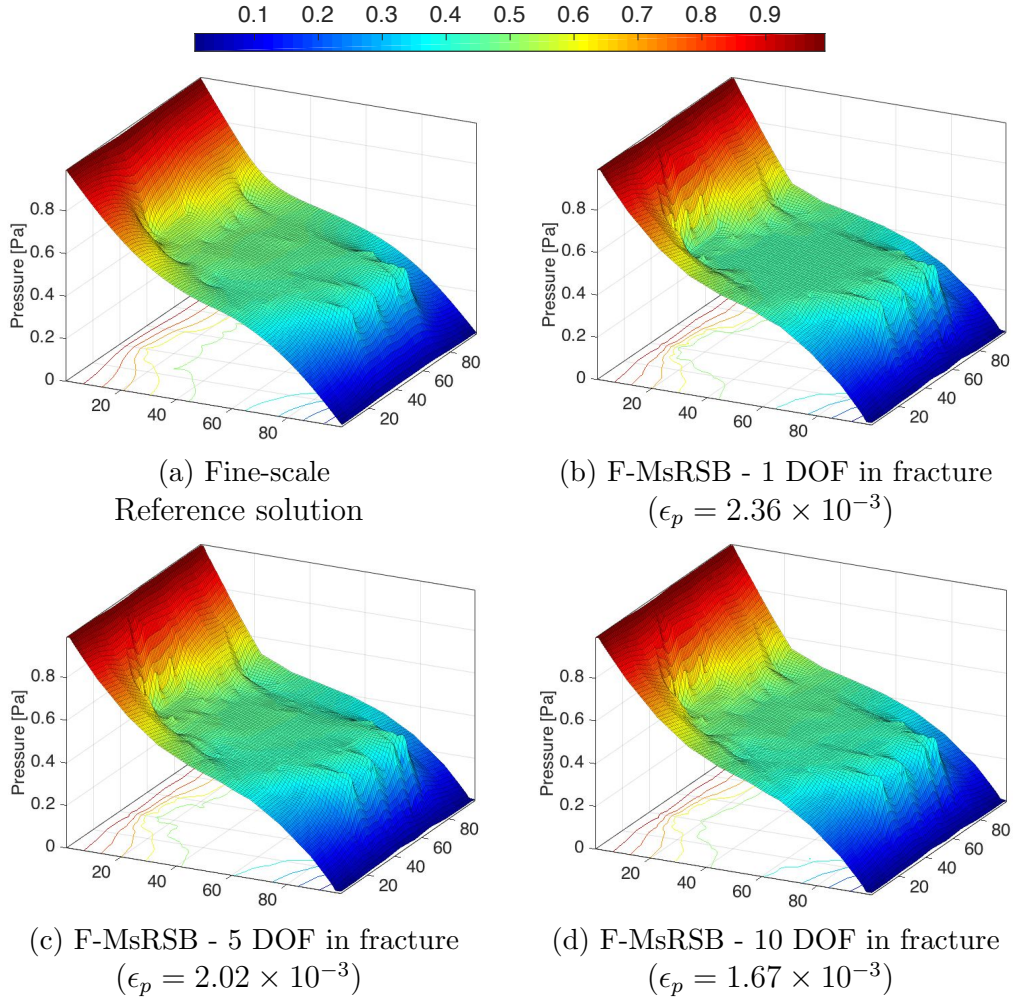


Fig. 8. Reference and F-MsRSB pressure for the first test case as shown in **Fig. 6**. F-MsRSB solutions are presented for different fracture coarsening ratios.

We consider two-phase flow, with quadratic relative permeability curves and unit viscosity ratio between the phases. Fluid is injected at a constant rate in cell (1,100), while fluids are produced in the opposite corner (100,1) at constant pressure. **Fig. 13** shows the saturation maps obtained after one F-MsRSB cycle (no iterations) compared with reference fine-scale solutions, both obtained using a sequentially-implicit strategy. Clearly, the higher the resolution of fracture coarse grid, the more accurate the F-MsRSB results.

Saturation error is calculated as

$$\epsilon_S = \frac{\max_{i \in n_f} (|S_i^{fs} - S_i^{ms}| |\Omega_i| \phi_i)}{\max_{i \in n_f} (|S_i^{fs}| |\Omega_i| \phi_i)}, \quad (26)$$

which, because it is scaled with pore volume, gives a very strict measure of the error in the spatial mass distribution for incompressible fluids.

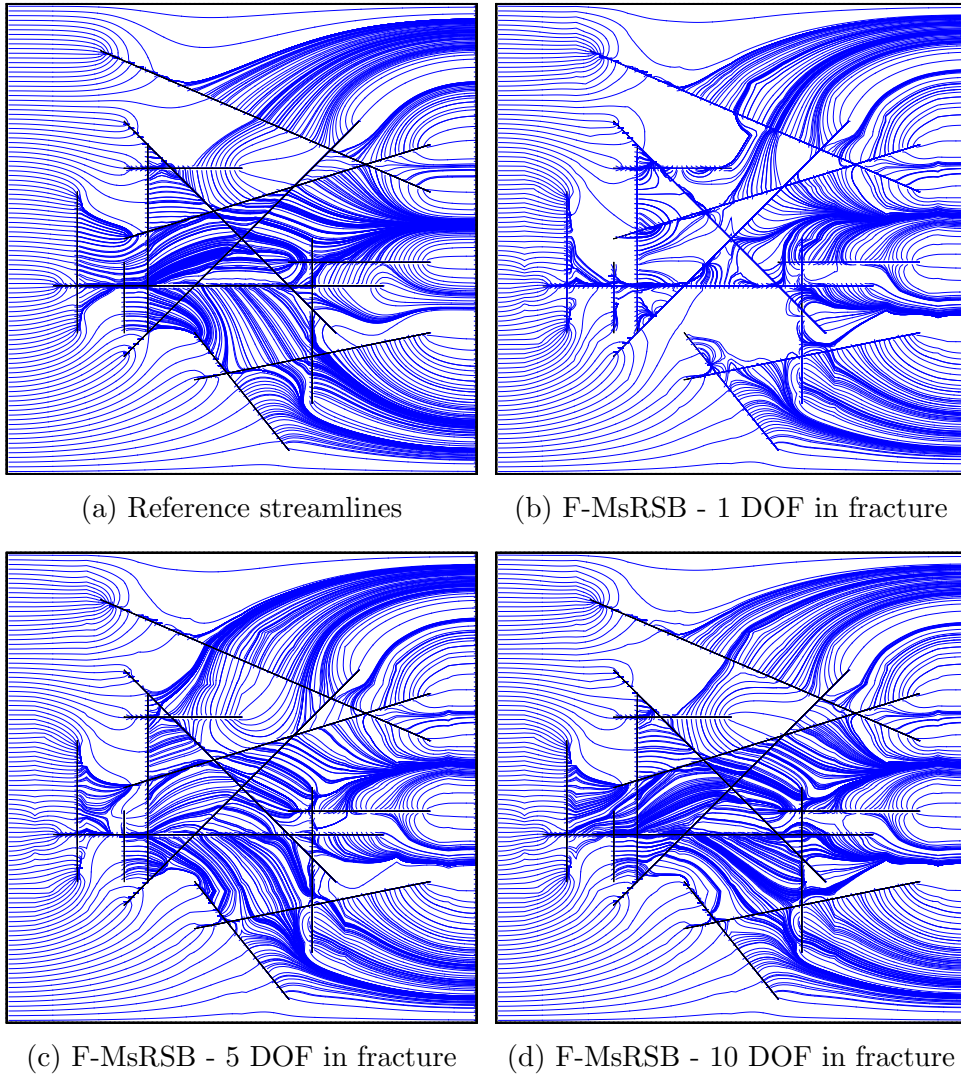


Fig. 9. Reference and F-MsRSB velocity field represented by streamlines for the first test case as shown in **Fig. 6**. F-MsRSB solutions are presented for different fracture coarsening ratios.

Clearly, multiscale solutions can be improved by increasing the number of degrees-of-freedom per fracture network or by applying iterations (in combination with ILU(0), similar to [50,58,47,53]). **Fig. 14** shows overall saturation errors. After only a few iterations of the two stage (F-MsRSB + ILU(0)) cycle, the multiscale fluid distribution is virtually identical to the reference solution. Convergence to a tolerance of 0.1 takes 8 iterations for this outcrop model, whereas a tolerance of 0.01 is reached after 20 iterations. One can also employ a local block solver around the fractures and wells [9].

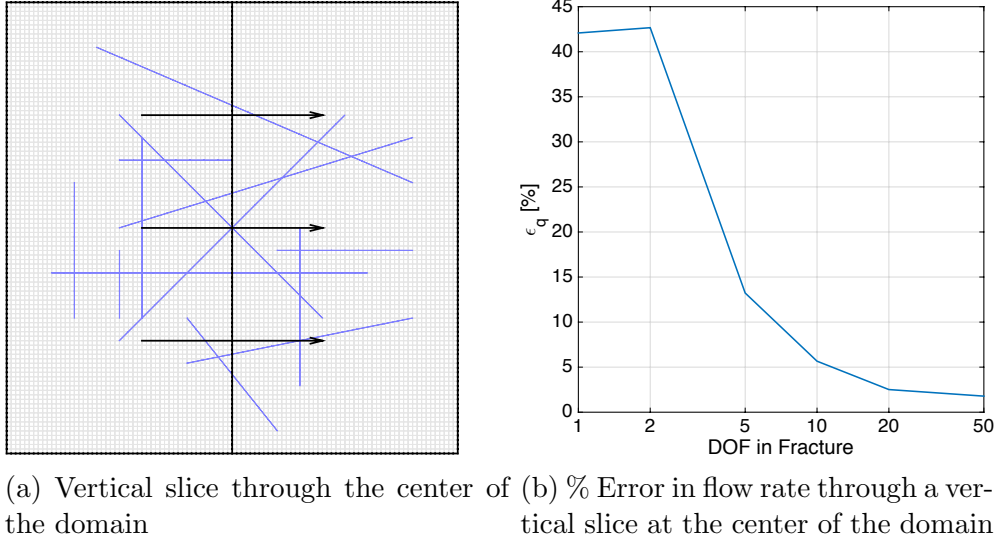


Fig. 10. Vertical cross section through the center of the matrix domain (a). Percentage error in total flow rate through this vertical cross section in the matrix (b).

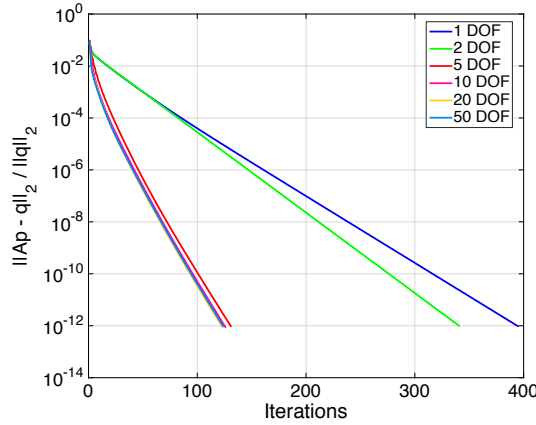


Fig. 11. Convergence of F-MsRSB+ILU(0) for different DOF in fracture.

5.2.2 Statistical fracture model

A $1000 \times 500 \text{ m}^2$ heterogeneous domain with permeability and porosity sampled from the 10-th layer of the SPE10 dataset [56] is considered and shown in **Fig. 15**. Similar as in previous test case, fracture permeability and porosity are 1000 Darcy and 0.50, respectively. PEBI grids are employed for the matrix at fine scale, which is a Voronoi map over a uniform triangulation in the region. The fine-scale grid contains 4726 cells for matrix and 2207 cells for fractures. There exist 55 disconnected fracture networks in the domain. Both matrix and fracture are coarsened using METIS [57] to give 100 blocks for each domain (fracture and matrix) as shown in **Fig. 15a**.

Two incompressible fluid phases with quadratic relative permeabilities are considered. The reservoir is initially filled with oil having a viscosity of 5 cP.

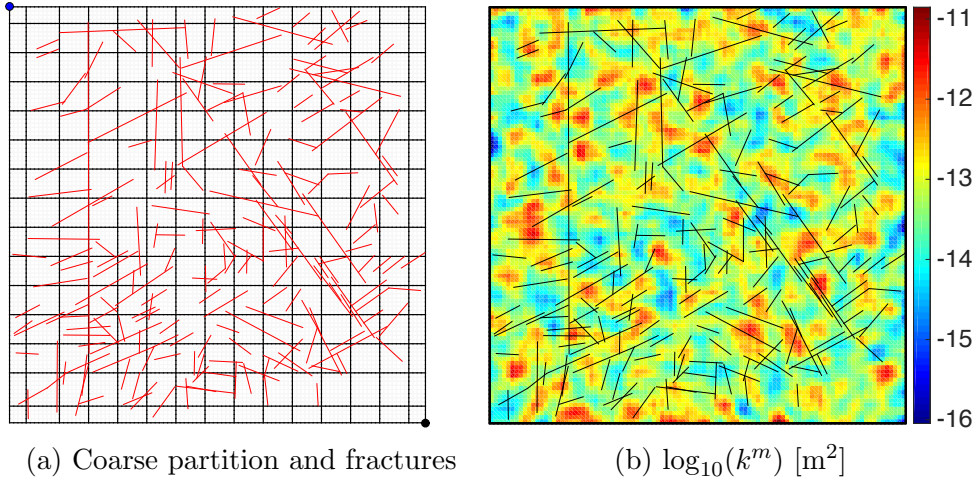


Fig. 12. Coarse grid in matrix showing well locations and fracture map extracted from an outcrop (a). Logarithm of the corresponding permeability field in the matrix (b).

Water with a lower viscosity of 1 cP is injected at a constant rate from a well near the bottom-left corner, while a the producing well near the top right corner of the domain is kept at constant pressure. **Fig. 16** shows the saturation maps after one multiscale cycle (F-MsRSB + ILU(0)) for injection amounts of 0.2, 1.0, and 1.8 pore volumes (PVI). The initial multiscale solution is already quite accurate, and after one smoothing-iteration step, the multiscale and reference solutions are virtually identical. **Fig. 17** compares bottom-hole pressure in the injector oil rate in the producer as computed by the fine-scale reference solver and F-MsRSB with different iterative tolerances.

5.3 3D models

In this section, we study the performance of F-MsRSB for three examples in which the matrix domain is described in 3D and fractures are planar 2D surfaces.

5.3.1 Two intersecting fracture planes

The fine-scale grid for the first 3D example consists of $50 \times 50 \times 50$ matrix cells and two fracture planes, each with 100×30 fracture grid cells. The fracture planes cross in the middle of the domain, as shown in **Fig. 18a**. Fluid is injected at a constant rate at the bottom-left corner, while production takes place from the top-right corner. Matrix permeability is shown in **Fig. 18b**. The F-MsRSB grid contains $20 \times 20 \times 20$ matrix blocks, whereas each fracture plan is partitioned into 12×4 fracture blocks. Fracture permeability is set to 10^4 Darcy. The matrix coarsening ratio is chosen such that the effect of fracture

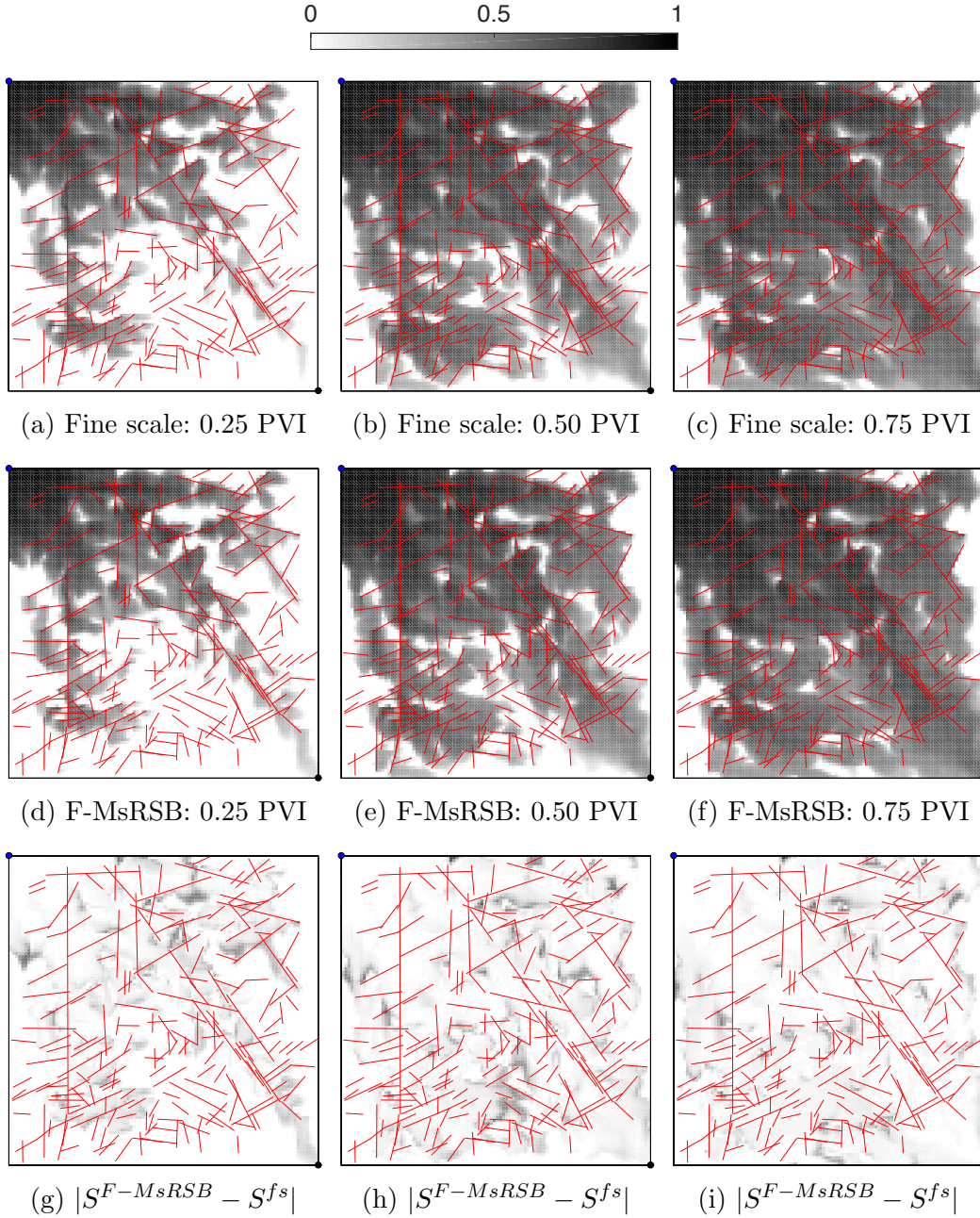


Fig. 13. Reference saturation profile compared with saturation maps obtained after one F-MsRSB cycle at different PV injected. Absolute errors in saturation are also shown in (g)-(i).

coarsening ratios will be more pronounced in the F-MsRSB results. **Fig. 19** shows the pressure solution obtained after one F-MsRSB step. In addition, **Fig. 20** presents the convergence behavior for different coarse resolutions for the fracture planes. We observe that a modest increase in the fracture resolution, from having a single DOF for each plane, leads to significantly improved convergence rates.

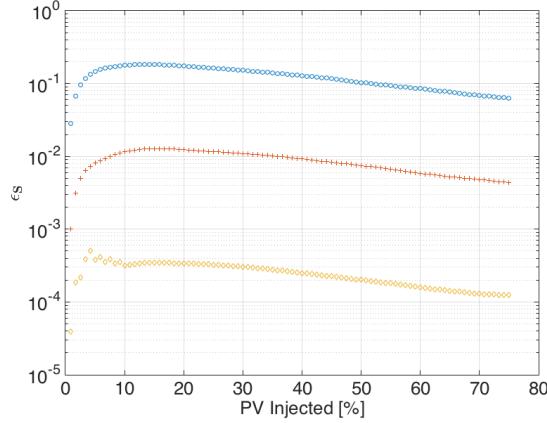
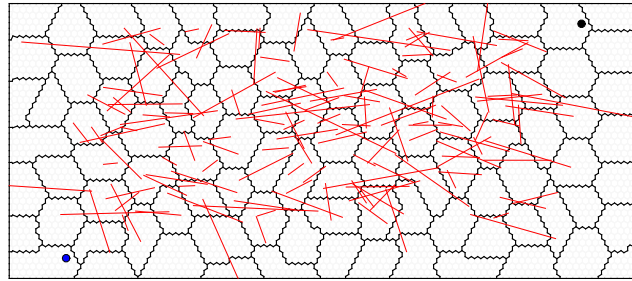


Fig. 14. Saturation error for the outcrop model as a function of simulation time measured in pore-volume-injection. Shown are the non-iterative and the iterative F-MsRSB method with tolerances of 0.1 and 0.01 on the pressure solves.



(a) Coarse grid with well locations

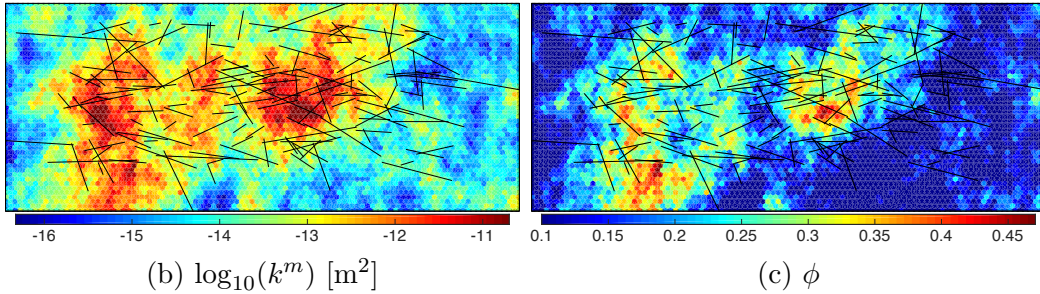


Fig. 15. Matrix coarse grid with 100 DOF, fracture map, and well locations (a). Petrophysical rock properties sampled from the 10th layer of the Tarbert formation in the SPE10 dataset (b and c).

5.3.2 Depositional bed

As another 3D example, we consider a corner-point grid modeling a core-scale depositional bed. A similar model has been used in the literature [8] as an example of a model with a large number of thin, low-permeable shale layers pinched between layers of good sands. Pinch-outs, owing mainly to erosion, are a common reason behind unstructured cell connections in stratigraphic corner-point grids. They lead to degenerate cells with faces of zero area resulting in a

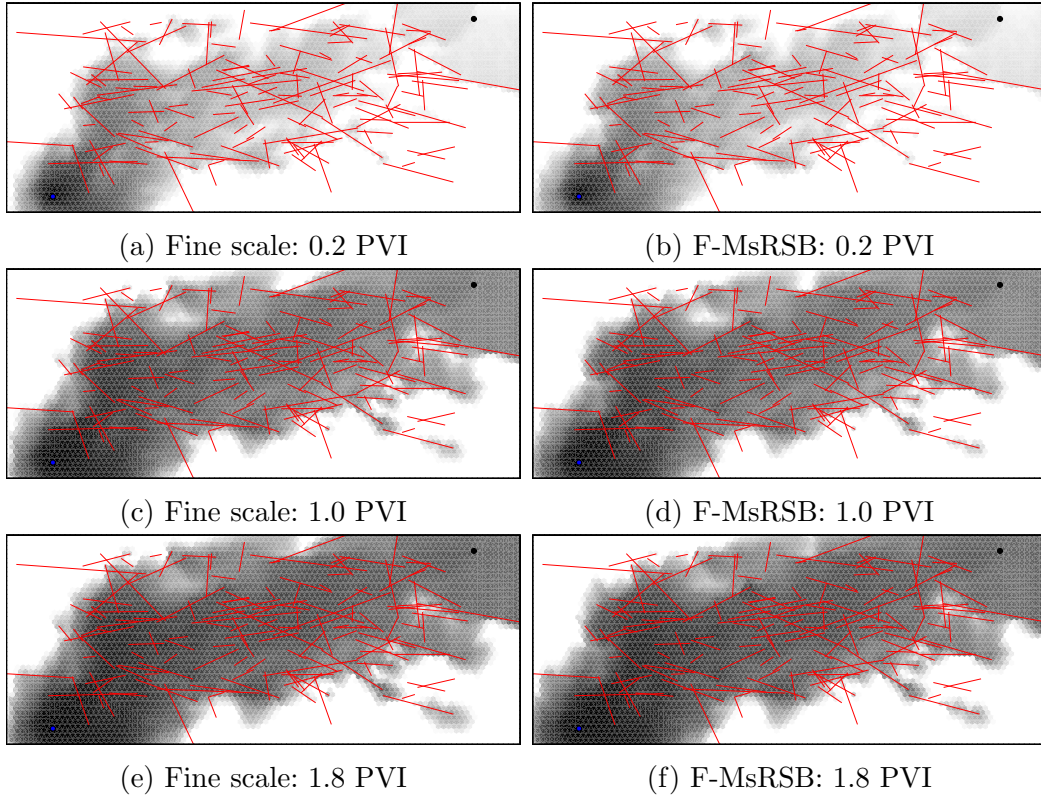


Fig. 16. Saturation maps at different times computed by the fine-scale reference solver and F-MsRSB with one iteration cycle (F-MsRSB + ILU(0)) .

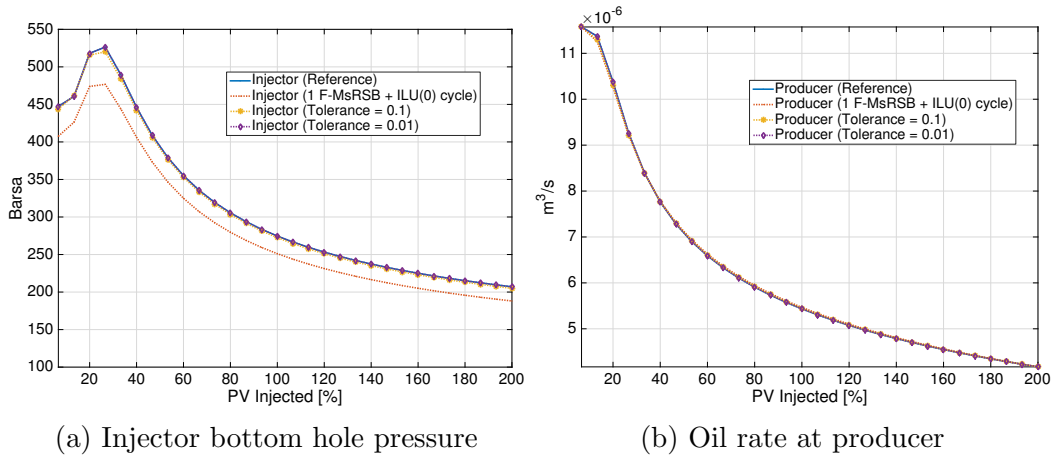


Fig. 17. Production and injection quantities at well locations for the statistical 2D fracture map.

complex grid geometry. With the addition of heterogeneity, it becomes quite a challenging test case for multiscale finite-volume methods [11,18]. We make the model even more complicated by adding inclined fracture planes in the interior of the model. To improve the efficiency of the F-MsRSB preprocessing steps for this challenging grid geometry, we first calculate the C_I factors globally for each fracture plane and then for each fracture-matrix overlapping discrete

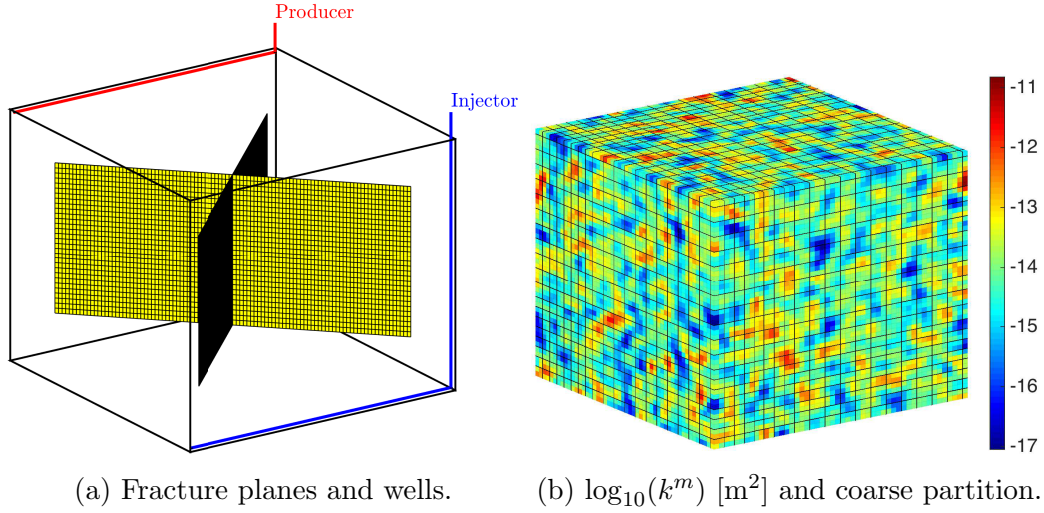


Fig. 18. Illustration of the first 3D test case, with a fine-scale grid that contains $50 \times 50 \times 50$ matrix cells and two intersecting fracture planes that each contain 100×30 fracture cells. Also shown on the right is heterogeneous matrix permeability map, along with the imposed $20 \times 20 \times 20$ coarse grid used by F-MsRSB.

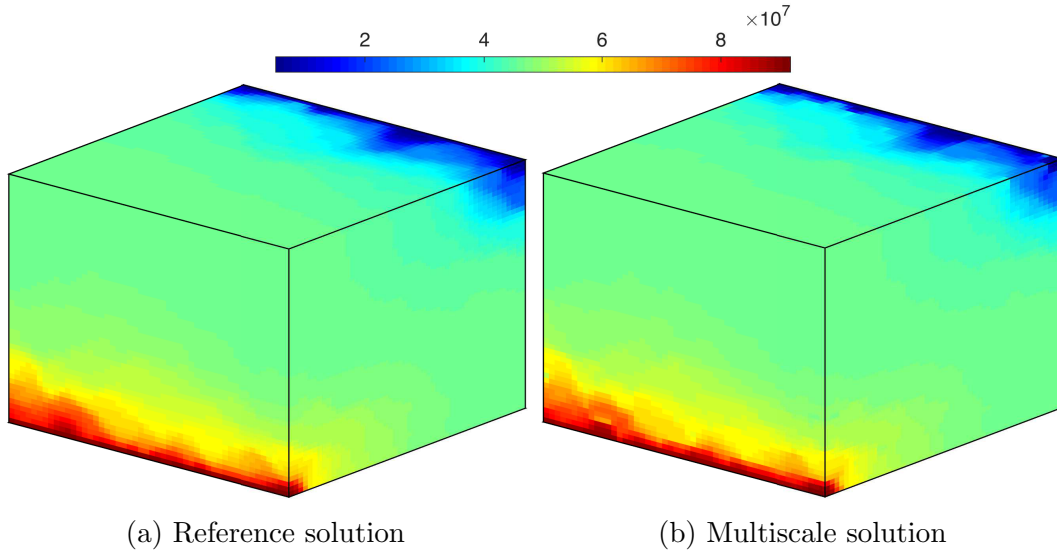


Fig. 19. Reference and multiscale pressure solution after one F-MsRSB cycle for single-phase flow in the simple 3D model. Each fracture plane is logically partitioned into 12×4 blocks.

grid cell.

The fine-scale grid contains $30 \times 30 \times 100$ matrix with 222 hexagonal fracture cells per fracture plane. As shown in **Fig. 21a**, there exist 6 fracture planes, and the domain is subject to Dirichlet boundary conditions on the left and right faces, while all other faces are subject to no-flow condition. As shown in **Fig. 21**, F-MsRSB employs $10 \times 10 \times 9$ blocks for the matrix rock, and only 2 blocks for each fracture plane. In addition, fracture aperture is $0.04m$. The matrix permeability distribution is shown in **Fig. 21b**, and we set $k_f = 10^4$

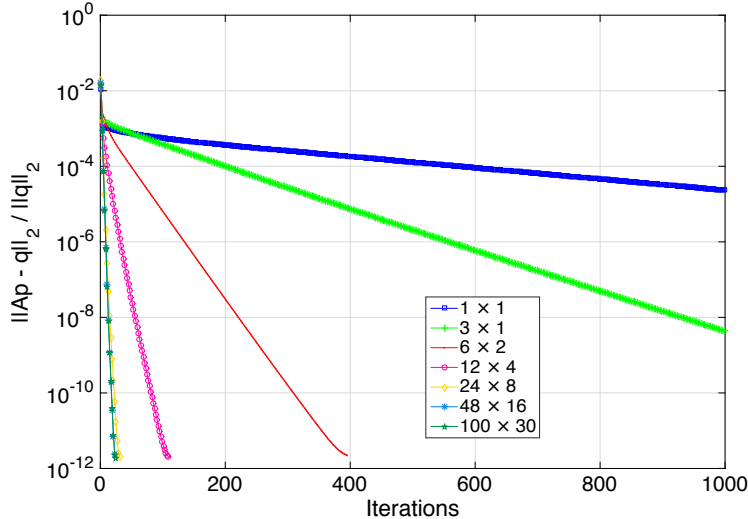


Fig. 20. Convergence property of the F-MsRSB + ILU (0) solver for various coarse resolutions of the two intersecting fracture planes, which each have 100×30 cells at the fine scale.

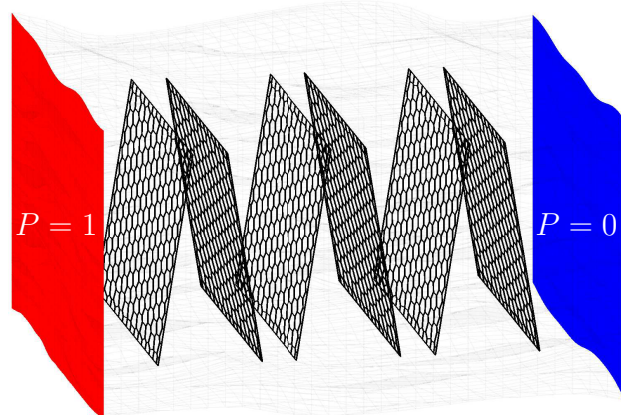
D, resulting in large contrasts in the permeability values throughout the entire model.

Fig. 22 shows pressure solutions obtained after one F-MsRSB step. It is clear that F-MsRSB and the fine-scale reference solutions are in good agreement, even with such a large coarsening ratio for the fractures. The absolute difference between the two solutions is depicted in **Fig. 22c**, with the pressure error (ϵ_p) being 8.79×10^{-4} .

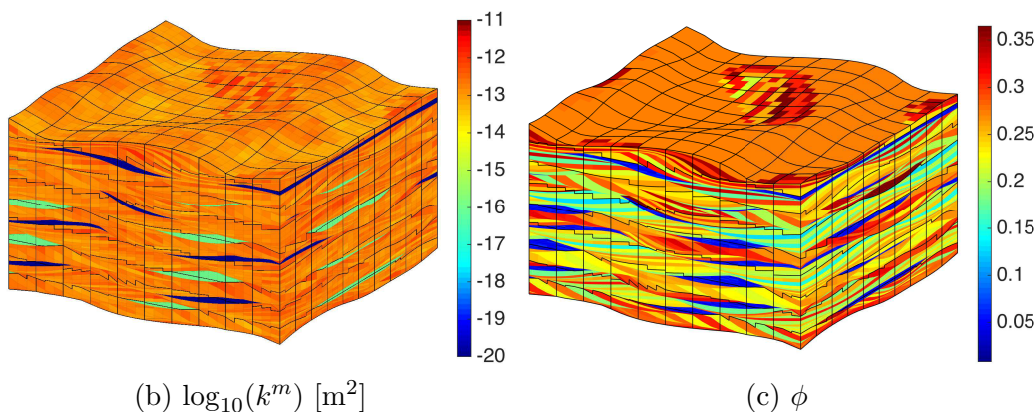
5.3.3 Model 2 of SPE10 with fracture networks

As the final test case in this section, we extract a $30 \times 110 \times 40$ subsample from the full 3D model of the challenging SPE10 data set [56]. As shown in **Fig. 23**, complex fracture planes (located between Layers 11 through 30) are obtained by extruding statistical maps, similar to the ones used for one of the 2D test cases. The model contains 31 disconnected fracture networks, which are discretized using 13,880 fine-scale grid cells.

Fig. 24 shows the matrix rock properties (permeability and porosity). All fractures have permeability value of 1000 Darcy. The coarse partitions used by F-MsRSB contain $6 \times 22 \times 8$ matrix and 181 fracture blocks in total. Each fracture block contains 80 fine-scale fracture cells. A waterflood experiment has been considered for the duration of 5 PVI, using quadratic relative permeability values. Water with viscosity 1 cP is injected into the reservoir, which is initially filled with 100% oil. Oil viscosity is 10 cP. As shown in **Fig. 23a**, five wells are placed in a five-spot pattern with a fixed rate injector in the middle and four fixed-pressure producers at the corners.



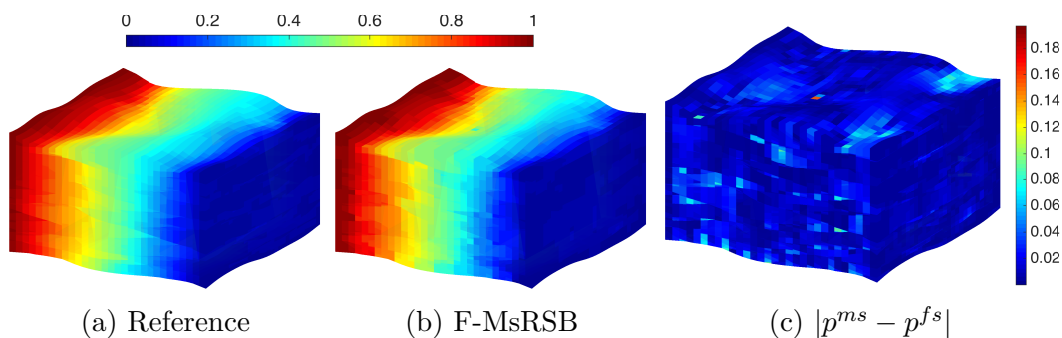
(a) Model outline, fractures, and boundary conditions



(b) $\log_{10}(k^m)$ [m^2]

(c) ϕ

Fig. 21. Matrix grid with fracture planes and boundary conditions (a). Logarithm of permeability map (b) and matrix porosity (c)



(a) Reference

(b) F-MsRSB

(c) $|p^{ms} - p^{fs}|$

Fig. 22. Reference and multiscale pressure solution for single-phase flow in the bed model with two degrees-of-freedom per fracture plane.

Well responses computed by F-MsRSB are presented in **Fig. 25** and compared with a fine-scale reference solution. As shown, one iteration of (F-MsRSB+ILU(0)) leads to significantly improved solutions. The initial multiscale solution residual is approximately 0.1, which reduces to approximately 0.01 after only one smoothing iteration. Convergence to a tolerance of 10^{-3} and subsequently to 10^{-4} takes approximately 5 and 15 iterations on average, respectively, per time step.

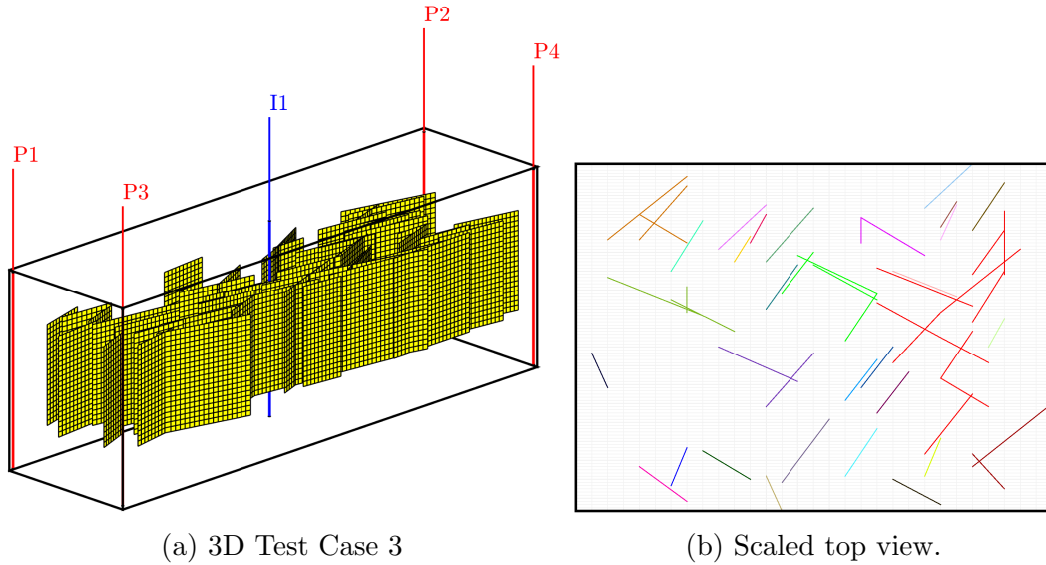


Fig. 23. Five-spot well locations in a subsample of the 3D SPE10 model with 31 disconnected fracture networks added. Shown on the right is the top view of the model.

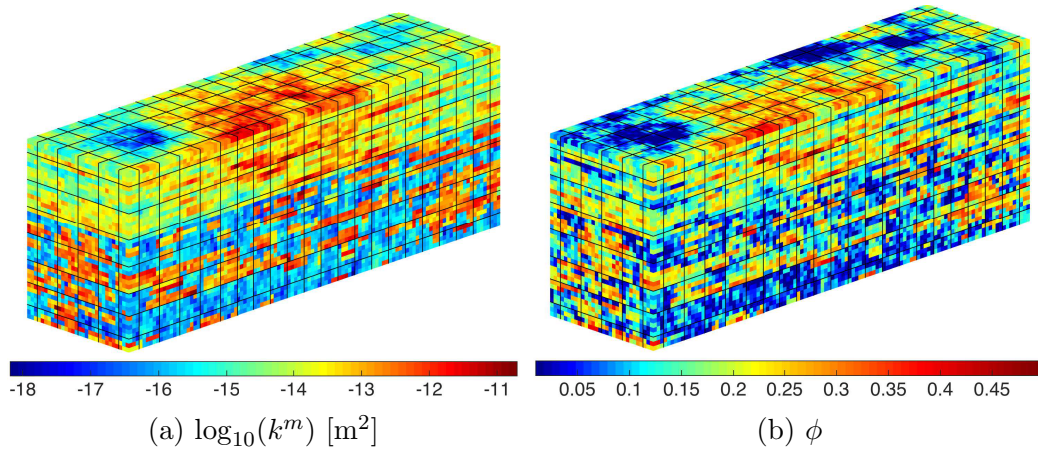


Fig. 24. Petrophysical properties for the $30 \times 110 \times 40$ domain sampled from the full SPE10 dataset

6 Conclusion

In this paper, a novel multiscale framework for fractured porous media (F-MsRSB) was introduced. The method benefited from the most recent developments within the multiscale community, namely F-AMS and MsRSB, and yet, devised a novel approach for robust and efficient treatments of fractured media. Efficiency and accuracy of the devised multiscale method was analyzed for many challenging test cases, including a realistic fracture map from an outcrop. These extensive studies are quite unique in the multiscale community. F-MsRSB is formulated and implemented in an algebraic form using the open-source MATLAB Reservoir Simulation Toolbox (MRST). The codes

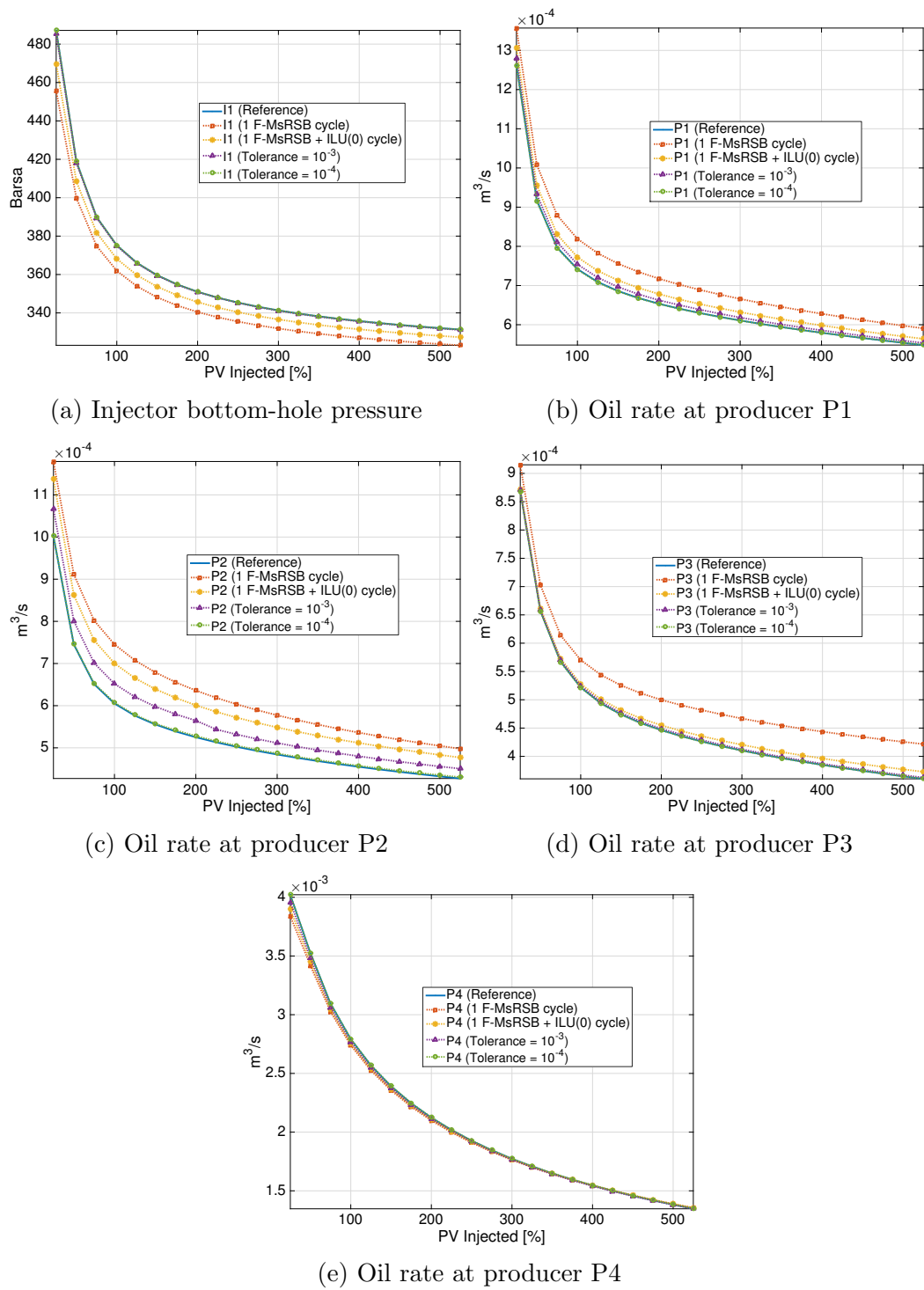


Fig. 25. Well responses for all wells of the 3D SPE10 test case.. F-MsRSB solutions are shown for different tolerances of pressure solution, compared with a fine-scale reference solution.

necessary to run the type of experiments reported herein are thus open to the scientific community; another important contribution of this work.

Through a set of single- and multiphase test cases it was found that MsRSB can accurately simulate models of fractured porous media with highly heterogeneous coefficients and produce approximate solutions with a prescribed fine-scale residual accuracy. The numerical test cases also included complex wells. By using an adaptive iterative strategy, one can trade accuracy for computational efficiency, and still produce mass-conservative, approximate solutions on the fine scale.

The basis functions used in this method can be adaptively updated using efficient global smoothing strategies to account for compressibility and gravity among other physical effects. Ongoing research includes consideration of more challenging fluid and rock physics, along with integration of F-MsRSB into an in-house C++ simulator for comparisons of CPU efficiency.

Acknowledgements

This work was sponsored in part by the Chevron/Schlumberger INTERSECT Technology Alliance and Schlumberger Petroleum Services CV, and in part by Schlumberger Information Solutions and the Research Council of Norway under grant no. 226035. [Matei Tene was sponsored by PI/ADNOC.](#)

References

- [1] K. Aziz, A. Settari, Petroleum Reservoir Simulation. Blitzprint Ltd., Calgary, Alberta, 1979.
- [2] T. Y. Hou, X.-H. Wu, A multiscale finite element method for elliptic problems in composite materials and porous media. *J. Comput. Phys.*, 134 (1997) 169–189.
- [3] P. Jenny, S. H. Lee, H. A. Tchelepi, Multi-scale finite-volume method for elliptic problems in subsurface flow simulation. *J. Comput. Phys.*, 187 (2003) 47–67.
- [4] P. Jenny, S. H. Lee, H. A. Tchelepi, Adaptive fully implicit multi-scale finite-volume method for multi-phase flow and transport in heterogeneous porous media. *J. Comput. Phys.*, 217 (2006) 627–641.
- [5] Y. Efendiev, T. Y. Hou, Multiscale Finite Element Methods: Theory and Applications. Springer, 2009.
- [6] V. Kippe, J. E. Aarnes, K.-A. Lie, A comparison of multiscale methods for elliptic problems in porous media flow. *Comput. Geosci.*, 12 (2008) 377–398.

- [7] J. E. Aarnes, V. Kippe, K.-A. Lie. Mixed multiscale finite elements and streamline methods for reservoir simulation of large geomodels. *Adv. Water Resour.*, 28 (2005) 257–271.
- [8] J. E. Aarnes, S. Krogstad, K.-A. Lie. Multiscale mixed/mimetic methods on corner-point grids. *Comput. Geosci.*, 12 (2008) 297–315.
- [9] H. Hajibeygi, P. Jenny. Adaptive iterative multiscale finite volume method. *J. Comput. Phys.*, 230 (2011) 628–643.
- [10] I. Lunati, P. Jenny, Multiscale finite-volume method for density-driven flow in porous media. *Comput. Geosci.*, 12 (2008) 337–350.
- [11] O. Møyner, K.-A. Lie. A multiscale two-point flux-approximation method. *J. Comput. Phys.*, 275 (2014) 273–293.
- [12] H. Hajibeygi, R. Deb, P. Jenny. Multiscale finite volume method for non-conformal coarse grids arising from faulted porous media. *Proceedings of SPE Reservoir Simulation Symposium*, (2011), DOI: 10.2118/142205-MS.
- [13] Y. Wang, H. Hajibeygi, H. A. Tchelepi. Monotone multiscale finite volume method. *Comput. Geosci.*, (2015) 1–16.
- [14] H. Hajibeygi, P. Jenny. Multiscale finite-volume method for parabolic problems arising from compressible multiphase flow in porous media. *J. Comput. Phys.*, 228 (2009) 5129–5147.
- [15] H. Zhou, H. A. Tchelepi. Operator based multiscale method for compressible flow. *SPE J.*, 13 (2008) 267–273.
- [16] P. Jenny, I. Lunati. Modeling complex wells with the multi-scale finite volume method. *J. Comput. Phys.*, 228 (2009) 687–702.
- [17] S. H. Lee, H. Zhou, H. Tchelepi. Adaptive multiscale finite-volume method for nonlinear multiphase transport in heterogeneous formations. *J. Comput. Phys.*, 228 (2009) 9036–9058.
- [18] O. Møyner, K.-A. Lie. The multiscale finite-volume method on stratigraphic grids. *SPE J.*, 19 (2014) 816–831.
- [19] H. Hajibeygi, S. H. Lee, I. Lunati. Accurate and efficient simulation of multiphase flow in a heterogeneous reservoir by using error estimate and control in the multiscale finite-volume framework. *SPE J.*, 17 (2012) 1071–1083.
- [20] H. Hajibeygi, G. Bonfigli, M. A. Hesse, P. Jenny. Iterative multiscale finite-volume method. *J. Comput. Phys.*, 227 (2008) 8604–8621.
- [21] H. Zhou, H. A. Tchelepi. Two-stage algebraic multiscale linear solver for highly heterogeneous reservoir models. *SPE J.*, 17 (2012) 523–539.
- [22] Y. Wang, H. Hajibeygi, H. A. Tchelepi. Algebraic multiscale linear solver for heterogeneous elliptic problems. *J. Comput. Phys.*, 259 (2014) 284–303.

- [23] M. Tene, Y. Wang, H. Hajibeygi. Adaptive algebraic multiscale solver for compressible flow in heterogeneous porous media. *J. Comp. Phys.*, 300 (2015) 679–694.
- [24] U. Trottenberg, C.W. Oosterlee, A. Schueller. *Multigrid*. Elsevier Academic Press, 2001.
- [25] S. H. Lee, C. Wolfsteiner, H. A. Tchelepi. Multiscale finite-volume formulation for multiphase flow in porous media: black oil formulation of compressible, three-phase flow with gravity. *Comput. Geosci.*, 12 (2008) 351–366.
- [26] H. Hajibeygi, H. A. Tchelepi. Compositional multiscale finite-volume formulation. *SPE J.*, 19 (2014) 316–326.
- [27] O. Møyner, K.-A. Lie. The multiscale finite volume method on unstructured grids. *Proceedings of SPE Reservoir Simulation Symposium*, (2014), DOI: 10.2118/163649-MS.
- [28] M. Cusini, A. Lukyanov, J. Natvig, H. Hajibeygi. Constrained pressure residual multiscale (CPR-MS) method for fully implicit simulation of multiphase flow in porous media. *J. Comp. Phys.*, 299 (2015) 472–486.
- [29] G. Barenblatt, Y. Zheltov, I. Kochina. Basic concepts in the theory of seepage of homogeneous fluids in fissurized rocks. *J. Appl. Math. Mech.*, 5 (1983) 1286–1303.
- [30] J. Warren, P. Root. The behavior of naturally fractured reservoirs. *SPE J.*, 3 (1963) 245–255.
- [31] H. Kazemi. Pressure transient analysis of naturally fractured reservoirs with uniform fracture distribution. *SPE J.*, 9 (1969) 451–462.
- [32] L. K. Thomas, T. N. Dixon, R. G. Pierson. Fractured reservoir simulation. *SPE J.*, 23 (1983) 42–54.
- [33] R. Baca, R. Arnett, D. Langford. Modeling fluid flow in fractured porous rock masses by finite element techniques. *Int. J. Num. Meth. Fluids*, 4 (1984) 337–348.
- [34] S. H. Lee, M. F. Lough, C. L. Jensen. Hierarchical modeling of flow in naturally fractured formations with multiple length scales. *Water Resources Research*, 37 (2001) 443–455.
- [35] S. H. Lee, C. L. Jensen, M. F. Lough. Efficient finite-difference model for flow in a reservoir with multiple length-scale fractures. *SPE J.*, 3 (2000) 268–275.
- [36] L. Li, S. H. Lee. Efficient field-scale simulation of black oil in naturally fractured reservoir through discrete fracture networks and homogenized media. *SPE Res. Eval. Eng.*, 11 (2008) 750–758.
- [37] J. R. Natvig, B. Skaflestad, F. Bratvedt, K. Bratvedt, K.-A. Lie, V. Laptev, S.K. Khataniar. Multiscale mimetic solvers for efficient streamline simulation of fractured reservoirs. *SPE J.*, 16 (2009) 880–888.

- [38] A. F. Gulbransen, V. L. Hauge, K.-A. Lie. A multiscale mixed finite element method for vuggy and naturally fractured reservoirs. *SPE J.*, 15 (2010) 395–403.
- [39] T. Barkve, A. Firoozabadi. Analysis of reinfiltration in fractured porous media. *Proceedings of SPE Annual Technical Conference and Exhibition*, (1992), DOI: 10.2118/24900-MS.
- [40] J. Noorishad, M. Mehran. An upstream finite element method for solution of transient transport equation in fractured porous media. *Water Resour. Res.*, 3 (1982) 588–596.
- [41] M. Karimi-Fard, A. Firoozabadi. Numerical simulation of water injection in 2D fractured media using discrete-fracture model. *Proceedings of SPE annual technical conference and exhibition*, (2001), DOI: 10.2118/71615-MS.
- [42] M. Karimi-Fard, L. J. Durlofsky, K. Aziz. An efficient discrete-fracture model applicable for general-purpose reservoir simulators. *SPE J.*, 9 (2004) 227–236.
- [43] A. Moinfar, A. Varavei, K. Sepehrnoori, R. T. Johns. Development of a coupled dual continuum and discrete fracture model for the simulation of unconventional reservoirs. *Proceedings of SPE Reservoir Simulation Symposium*, (2013), DOI: 10.2118/163647-MS
- [44] R. Ahmed, M.G. Edwards, S. Lamine, B.A.H. Huisman, M. Pal. Control-volume distributed multi-point flux approximation coupled with a lower-dimensional fracture model. *J. Comput. Phys.*, 284 (2015) 462–489.
- [45] H. Hajibeygi. *Iterative multiscale finite-volume method for multiphase flow in porous media with complex physics*. Phd thesis, ETH Zurich, Switzerland, 2011.
- [46] A. Moinfar, K. Sepehrnoori, R. T. Johns, A. Varavei. Coupled geomechanics and flow simulation for an embedded discrete fracture model. *Proceedings of SPE Reservoir Simulation Symposium*, (2013), DOI: 10.2118/163666-MS
- [47] H. Hajibeygi, D. Karvounis, P. Jenny, A hierarchical fracture model for the iterative multiscale finite volume method. *J. Comput. Phys.*, 230 (2011) 8729–8743.
- [48] I. S. Ligaarden, M. Krokiewski, K.-A. Lie, D. W. Schmid, M. Pal. On the Stokes–Brinkman equations for modeling flow in carbonate reservoirs. *Proceedings of ECMOR XII–12th European Conference on the Mathematics of Oil Recovery*, (2010), DOI: 10.3997/2214-4609.20144924
- [49] T. H. Sandve, I. Berre, E. Keilegavlen, J. M. Nordbotten. Multiscale simulation of flow and heat transport in fractured geothermal reservoirs: inexact solvers and improved transport upscaling. *Proceedings of Thirty-Eighth Workshop on Geothermal Reservoir Engineering*, (2013), Stanford University, USA.
- [50] M. Tene, M. S. Al Kobaisi, H. Hajibeygi. Algebraic multiscale solver for flow in heterogeneous fractured porous media. *Proceedings of SPE Reservoir Simulation Symposium*, (2015), DOI: 10.2118/173200-MS.

- [51] M. Tene, M. S. Al Kobaisi, H. Hajibeygi. Algebraic multiscale solver for fractured porous media (F-AMS). *J. Comp. Phys.* (2015). in review.
- [52] O. Møyner, K.-A. Lie. A multiscale method based on restriction-smoothed basis functions suitable for general grids in high contrast media. *Proceedings of SPE Reservoir Simulation Symposium*, (2015), DOI: 10.2118/173265-MS.
- [53] O. Møyner, K.-A. Lie. A multiscale restriction-smoothed basis method for high contrast porous media represented on unstructured grids. *J. Comput. Phys.*, 304 (2015) 46 - 71, DOI: 10.1016/j.jcp.2015.10.010.
- [54] O. Møyner, K.-A. Lie. A multiscale restriction-smoothed basis method for compressible black-oil models. *SPE J.*, (2016). to appear.
- [55] S. T. Hilden, O. Møyner, K.-A. Lie, K. Bao. Multiscale simulation of polymer flooding with shear effects. (2016). to appear.
- [56] M. A. Christie, M. J. Blunt. Tenth SPE comparative solution project: A comparison of upscaling techniques. *SPE Res. Eval. Eng.*, 4 (2001) 308–317.
- [57] G. Karypis, V. Kumar. A fast and high quality multilevel scheme for partitioning irregular graphs. *SIAM J. Sci. Comput.*, 20 (1998) 359–392.
- [58] Y. Wang, H. Hajibeygi, H. A. Tchelepi. Algebraic multiscale solver for flow in heterogeneous porous media. *J. Comput. Phys.*, 259 (2014) 284–303.
- [59] Y. Saad. *Iterative Methods for Sparse Linear Systems*. SIAM, USA, 2003.
- [60] The MATLAB Reservoir Simulation Toolbox (MRST), version 2015a. SINTEF Applied Mathematics, May 2015.
- [61] K.-A. Lie. *An Introduction to Reservoir Simulation Using MATLAB: User guide for the Matlab Reservoir Simulation Toolbox (MRST)*. SINTEF ICT, <http://www.sintef.no/Projectweb/MRST/publications>, 2nd edition, Dec 2015.
- [62] L. S. K. Fung, A. H. Dogru. Distributed unstructured grid infrastructure for complex reservoir simulation. *Proceedings of Europec/EAGE Conference and Exhibition*, (2008), DOI: 10.2118/113906-MS.
- [63] A. Kozlova, Z. Li, J. R. Natvig, S. Watanabe, Y. Zhou, K. Bratvedt, S. H. Lee. A real-field multiscale black-oil reservoir simulator. *Proceedings of SPE Reservoir Simulation Symposium*, (2015), DOI: 10.2118/173226-MS
- [64] P. Vanek, J. Mandel, M. Brezina. Algebraic multigrid by smoothed aggregation for second and fourth order elliptic problems. *Computing*, 56 (1996) 179–196.
- [65] P. Vanek. Acceleration of convergence of a two-level algorithm by smoothing transfer operator. *Appl. Math.*, 37 (1992) 265–274.
- [66] H. Guillard, P. Vanek. An aggregation multigrid solver for convection-diffusion problems on unstructured meshes. Technical report, Center for Computational Mathematics, University of Colorado at Boulder, 1998.

- [67] K.-A. Lie, S. Krogstad, I. S. Ligaarden, J. R. Natvig, H. M. Nilsen, B. Skaflestad. Open-source matlab implementation of consistent discretisations on complex grids. *Comput. Geosci.*, 16 (2012) 297–322.
- [68] S. Krogstad, K.-A. Lie, O. Møyner, H. M. Nilsen, X. Raynaud, B. Skaflestad. MRST-AD – An open-source framework for rapid prototyping and evaluation of reservoir simulation problems. *Proceedings of SPE Reservoir Simulation Symposium*, (2015), DOI: 10.2118/173317-MS.
- [69] K. Bisdom, B. D. M. Gauthier, G. Bertotti, N. J. Hardebol. Calibrating discrete fracture-network models with a carbonate three-dimensional outcrop fracture network: Implications for naturally fractured reservoir modeling. *AAPG Bulletin*, 24 (2014) 1351-1376.
- [70] D. W. Pollock. Semianalytical computation of path lines for finite-difference models. *Ground water*, 26 (1988) 743-750.